OPTICAL STIMULATION OF THE PROSTATE NERVES: A POTENTIAL DIAGNOSTIC TECHNIQUE

by

Serhat Tozburun

A dissertation submitted to the faculty of
The University of North Carolina at Charlotte
in partial fulfillment of the requirements
for the degree of Doctor of Philosophy in
Optical Science and Engineering

Charlotte

2012

Approved by:

_____
Dr. Nathaniel M. Fried

_____
Dr. Michael A. Fiddy

_____
Dr. Eric G. Johnson

_____
Dr. Faramarz Farahi

_____
Dr. Mark G. Clemens

ABSTRACT

SERHAT TOZBURUN. Optical stimulation of the prostate nerves: a potential diagnostic technique. (Under the direction of DR. NATHENIEL M. FRIED)

There is wide variability in sexual potency rates (9 - 86%) after nerve-sparing prostate cancer surgery due to limited knowledge of the location of the cavernous nerves (CN's) on the prostate surface, which are responsible for erectile function. Thus, preservation of the CN's is critical in preserving a man's ability to have spontaneous erections following surgery.

Nerve-mapping devices, utilizing conventional Electrical Nerve Stimulation (ENS) techniques, have been used as intra-operative diagnostic tools to assist in preservation of the CN. However, these technologies have proven inconsistent and unreliable in identifying the CN's due to the need for physical contact, the lack of spatial selectivity, and the presence of electrical artifacts in measurements. Optical Nerve Stimulation (ONS), using pulsed infrared laser radiation, is studied as an alternative to ENS.

The objective of this study is sevenfold: (1) to develop a laparoscopic laser probe for ONS of the CN's in a rat model, in vivo; (2) to demonstrate faster ONS using continuous-wave infrared laser radiation; (3) to describe and characterize the mechanism of successful ONS using alternative laser wavelengths; (4) to test a compact, inexpensive all-single-mode fiber configuration for optical stimulation of the rat CN studies; (5) to implement fiber optic beam shaping methods for comparison of Gaussian and flat-top spatial beam profiles during ONS; (6) to demonstrate successful ONS of CN's through a thin layer of fascia placed over the nerve and prostate gland; and (7) to verify the

experimentally determined therapeutic window for safe and reliable ONS without thermal damage to the CN's by comparison with a computational model for thermal damage.

A 5.5-Watt Thulium fiber laser operated at 1870 nm and two pigtailed, single mode, near-IR diode lasers (150-mW, 1455-nm laser and 500-mW, 1550-nm laser) were used for non-contact stimulation of the rat CN's. Successful laser stimulation, as measured by an intracavernous pressure (ICP) response in the penis, was achieved with the laser operating in CW mode. CW optical nerve stimulation provides a significantly faster ICP response time using a lower laser power laser than conventional pulsed stimulation.

An all-single-mode fiber design was successfully tested in a rat model. The CN reached a threshold temperature of ~ 42 ^{o}C, with response times as short as 3 s, and ICP responses in the rat penis of up to 50 mmHg compared to a baseline of 5 - 10 mmHg. Chemical etching of the distal single-mode-fiber tip produced a concave shape and transformed the Gaussian to a flat-top spatial beam profile, resulting in simplified alignment of the laser beam with the nerve. This novel, all-single-mode-fiber laser nerve stimulation system introduces several advantages including: (1) a less expensive and more compact ONS configuration; (2) elimination of alignment and cleaning bulk optical components; and (3) improved spatial beam profile for simplified alignment.

For the fascia layers over the CN's (240 - 600 μm), the 1550 nm laser with an optical penetration depth of ~ 930 μm in water was substituted for the 1455 nm laser. Successful ONS was achieved, for the first time, in fascia layers up to 450 μm thick which is critical for future clinical translation of this method for intra-operative identification and preservation of CN's during prostate cancer surgery.

In order to define the upper limit of the therapeutic window for ONS of CN in a rat model, in vivo, identification of the thermal damage threshold for the CN after laser irradiation was investigated by direct comparison of the visible thermal damage data with a theoretical thermal damage calculation utilizing a standard Arrhenius integral model.

ACKNOWLEDGMENTS

This study is the result of my work as a research assistant in the Biomedical Optics Laboratory at the University of North of Charlotte in the years 2008 - 2012. None of this would have been possible without the generous help of many people whom I would like to thank.

First of all, I would like to thank my research supervisor Dr. Nathaniel M. Fried for his guidance, encouragement, continual support, and careful attention to the details involved in completing the Ph.D. study. I am deeply grateful to him for embarking with me on this thesis journey.

Special thanks go to Gwen A. Lagoda and Dr. Arthur L. Burnett, director of the Basic Science Laboratory in Neurology at Johns Hopkins Medical Institutions, Baltimore, MD, for their clinical assistance during all phases of the project.

I am deeply indebted to Dr. Faramarz Farahi for his suggestion and guidance in fiber optics beam shaping studies.

I would like to thank the other committee members, Dr. Michael A. Fiddy, Dr. Eric G. Johnson, Dr. Faramarz Farahi, and Dr. Mark G. Clemens, for following my research, taking their valuable time to read my thesis and offering detailed suggestions.

I also wish to thank all of my colleagues, Christopher M. Cilip, Richard L. Blackmon, Thomas C. Hutchens, and Yigit O. Yilmaz, at the university and all of my friends in Charlotte over the past five years for always being with me and their endless friendships. The group has been a source of friendships as well as good advice and collaboration.

This research was supported in part by the Department of Defense Prostate Cancer Research Program, Grant# PC073709, and the Department of Energy, Grant# DE-FG02-06CH11460. I was also supported in part by an Optics and Photonics Scholarship from the Society of Photo-Instrumentation Engineers (SPIE).

Of course, I owe my loving thanks to Lindsay A. Johnston for her presence, abundant confidence, understanding, deep love and continual support during the final stages of this Ph.D. study.

Lastly, and most importantly, I am grateful to my family, Seyit Tozburun, Güler Tozburun, Oğuzhan Tozburun and Batuhan Tozburun, for their endless encouragement, patience, continuing support, and love during my studies all which gives me the freedom to make my own decisions. I gratefully acknowledge for my parents who raised me with a love of science and supported me in all my pursuits.

It is to Oğuzhan Tozburun, who passed away on January 1, 2009 in an unlucky accident while celebrating New Year with his friends, I wish to dedicate this thesis.

TABLE OF CONTENTS

LIST OF TABLES

LIST OF FIGURES

LIST OF ABBREVIATIONS

CN’s	Cavernous nerves
ENS	Electrical Nerve Stimulation
ONS	Optical Nerve Stimulation
IR	Infrared
ICP	Intracavernous pressure
WD	Working distance
CW	Continuous-wave
ID	Inner diameter
OD	Outer diameter
NA	Numerical aperture
Ge	Germanium
F	Fluorine
HF	Hydrofluoric
DI	Distilled
UV	Ultraviolet
OPD	Optical penetration depth
SMF	All-single-mode fiber
SNR	Signal-to-noise ratio
OCT	Optical coherence tomography
$\Omega(t)$	Thermal damage parameter
ζ	Frequency factor
τ	total heating time

E_a	Activation energy
R	Universal gas constant
T	Absolute temperature
T_{crit}	Critical temperature

CHAPTER 1: INTRODUCTION

1.1 Cavernous Nerves

The Cavernous Nerves (CN's) are responsible for male sexual function. The CN's course in the neurovascular bundles along the surface of the prostatic capsule [1]. Because of the close proximity of the nerves to the prostate surface, they are at risk of injury during dissection and removal of a cancerous prostate gland.

In addition, many of these nerve fibers are microscopic, and vary in size among patients, making it difficult to predict the location and path of these nerves during prostate cancer surgery [2]. Therefore, preservation of the CN's is critical in preserving a man's ability to have spontaneous erections following surgery. Figure 1.1 shows a cross-sectional diagram and a photo of the human prostate showing the location of the neurovascular bundle and surgical dissection plane.

Erectile dysfunction, generally caused by injury of these nerves, is a common concern for patients and one of the major complications of prostate cancer surgery [3-4]. There is a wide variability in the recovery rate for erectile function of 9 - 86% following prostate cancer surgery [2]. Thus, development of improved methods for identification of the CN's and preservation of erectile function during surgery is important for providing a high quality-of-life for patients after prostate cancer treatment.

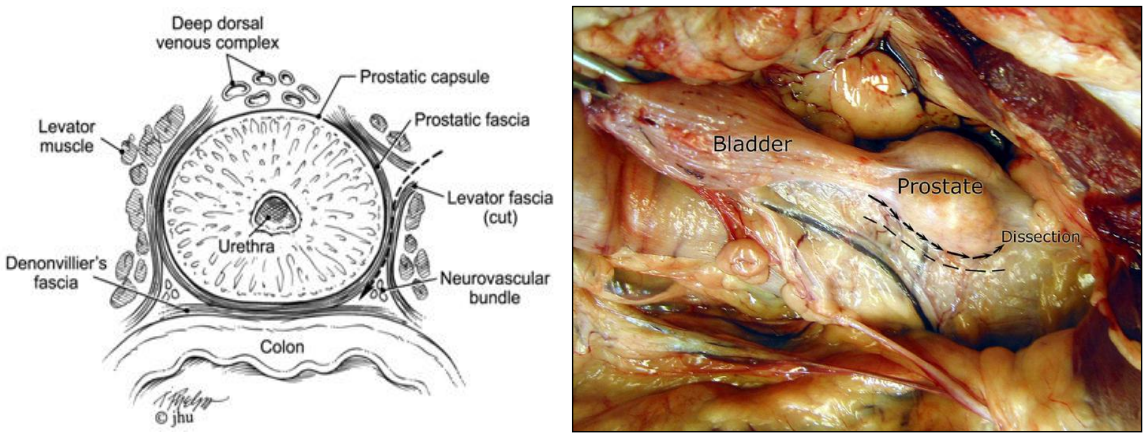

(a) (b)

Figure 1.1: (a) Cross-sectional diagram of the human prostate showing the location of the neurovascular bundle and its close proximity to the prostate surface. (b) Arrows indicate the surgical dissection plane and the dashed line indicates the position of the periprostatic neurovascular bundle under a superficial layer of fascia.

1.2 Electrical Nerve Stimulation

Conventional Electrical Nerve Stimulation (ENS) of the CN's is a common technique which uses an electrical current to stimulate neurons by initiating an action potential. ENS is used in both clinical and scientific studies to measure erectile response. The advantage of this technique is that the stimulation parameters (voltage, current, pulse duration, and repetition rate) can be controlled and measured [5]. Nerve mapping devices have also been used as intra-operative diagnostic tools to assist in preservation of the CN's during nerve-sparing prostate cancer surgery [6-9]. However, these nerve mapping technologies have proven inconsistent and unreliable in identifying the CN's and evaluating nerve function. There are several significant limitations of electrical nerve mapping techniques in general, including: lack of specificity, high false positive

responses, and the influence of multiple conflicting factors in recording an electrical response during surgery [7-9].

ENS in general has several major limitations. First, there is a need for physical contact between the electrodes and the nerve introducing the potential for mechanical damage. Second, there is a lack of spatial selectivity due to the limitation in size of the electrodes and electrical current spreading in tissue. Finally, there is a presence of electrical stimulation artifacts that may interfere with measurement.

1.3 Optical Nerve Stimulation

Recently, Optical Nerve Stimulation (ONS), using pulsed infrared (IR) laser radiation has been reported, as a potential alternative to ENS [10-16]. This novel nerve stimulation method may have significant advantages compared with ENS for both scientific studies and clinical applications. First, it is a non-contact method of stimulation because the IR laser radiation is delivered in a non-contact mode. Second, spatial selectivity is improved because the laser beam can be focused down smaller than a typical electrode and the problem of electrical current spreading out in the tissue is eliminated for ONS. Finally, when stimulating a nerve optically and measuring intracavernous pressure (ICP) responses electrically, or by another means, electrical stimulation artifacts are eliminated.

Successful ONS of the CN's in a rat model, in vivo, has been previously demonstrated [17-30]. However, there are significant limitations of ONS. First, a major limitation is a narrow therapeutic window of radiant exposures from 0.35 - 1.0 J/cm^2 for safe, reliable and reproducible nerve stimulation [10, 20, 31]. A radiant exposure less than this range may not produce a reliable erectile response, while a radiant exposure

higher than this range may cause thermal damage to the nerve upon repetitive stimulation, thus resulting in loss of sexual function.

Second, the beam diverges after exiting the output end of the optical fiber. Since the beam diameter increases as a function of distance due to beam divergence, providing a collimated laser beam is critical to produce a constant radiant exposure over a short working distance (WD) in a surgical environment, where the WD between the handheld probe tip and nerve surface may not be precisely controlled. In addition, it may also be important to use a flat-top spatial beam profile to produce a more uniform radiant exposure distribution than a typical Gaussian spatial beam profile over the nerve surface which is a delicate tissue structure, to avoid potential heat-induced nerve damage during ONS applications.

Third, the use of pulsed laser radiation at relatively low pulse repetition rates (2 - 13 Hz) for long-term ONS, presumably to avoid thermal build-up and thermal damage to the nerve, produces relatively slow nerve activity. However, rapid, short-term nerve stimulation will be required for the potential of ONS to be used as an intra-operative diagnostic tool, specifically for identification and preservation of the cavernous nerves during laparoscopic and robotic prostate cancer surgery. Delivery of the IR laser radiation to the nerve at significantly higher pulse rates (10 - 100 Hz) or in continuous-wave (CW) mode may result in a more rapid response for identification of the CN's.

Fourth, although the rat model is an ideal laboratory model for ONS studies, the cavernous nerve is directly visible on the surface of the prostate. However, the human CN's lay below a thin layer of periprostatic levator fascia, varying from 100 to 300 μm in thickness [32-34]. Thus, demonstrating successful subsurface ONS will be valuable for

the translation of ONS into the clinic as an intra-operative diagnostic tool for identification and preservation of the human CN's during prostate cancer surgery.

Chapter 2 provides details about the design and assembly of a laparoscopic probe for future testing in non-contact ONS of the CN in the clinic. There are basically two types of probes built for comparison; the first probe capable of delivering a collimated, 1-mm-diameter Gaussian laser beam, and the second probe producing a collimated, relatively flat-top spatial beam profile for uniform stimulation of the rat CN with a similar beam diameter as the first probe.

A comparison of CW and pulsed modes of delivery with varying pulse repetition rates, produced by a Thulium fiber laser at the wavelength of 1870 nm, is demonstrated in Chapter 3. The investigation in this study is focused on the evoked ICP response and response time from the CN in a rat model, in vivo. In addition, this chapter provides temperature measurements on the surface of the rat CN during IR laser stimulation, and provides insight into the photothermal mechanism of ONS.

A novel-single-mode-fiber design utilizing a 1455-nm diode laser was tested for ONS of CN in rat model, in vivo, and erectile responses in terms of ICP measurements are described in Chapter 4. In addition, a direct comparison for both Gaussian and flat-top spatial beam profiles was performed. Experimental setup and results are presented and discussed.

In Chapter 5, we explore feasibility of ONS of the rat CN with a fascia layer placed over the nerve on the prostate surface. Subsurface ONS of the rat CN's at a depth of 450 μm using a 1550-nm laser is demonstrated as an intermediate step towards ONS during prostate cancer surgery.

After investigating the biophysical mechanism and threshold for producing consistent and reliable ONS of the rat CN, we explore the threshold temperature for thermal damage to the nerve in Chapter 6. Experimental observations of nerve thermal damage are directly compared with a theoretical Arrhenius integral model of thermal damage.

CHAPTER 2: DESIGN AND ASSEMBLY OF OPTICAL NERVE STIMULATION PROBE

2.1 Introduction

In this chapter, we present the modeling and assembly of a laparoscopic probe for use in noncontact optical stimulation of the cavernous nerves (CN's) in a rat model, in vivo. Clinical application of Optical Nerve Stimulation (ONS) will require safe and reproducible results. In addition, optimization and characterization of the laser parameters and handheld laser probe design play a critical role in nerve stimulation because of the delicate structure of nerves.

First, two different laparoscopic laser probes, capable of delivering a 1-mm diameter laser beam, were built with a 200-μm-core multimode optical fiber (BFL22-200, Thorlabs, Newton, NJ) and with a standard single-mode optical fiber (9/125 μm, smf-28+, Corning Optical Fiber, Corning, NY), respectively. The multimode fiber assembled probe was used in the optical stimulation of the rat CN studies with a multimode Thulium fiber laser design (See Chapter 3). The probe consisting of a 9-μm-core single-mode fiber was used in similar animal studies with an all-single-mode fiber design (See Chapter 4).

Then, the single-mode fiber laser probe was modified to include a fiber optic beam shaping technique. A wet chemical etching technique was used to convert the Gaussian to flat-top spatial beam profile and provide more uniform irradiation across the nerve surface.

2.2 Conventional Gaussian Probe Design

A standard probe from an existing disposable laparoscopic instrument was used to house a miniature linear motorized stage (MM-3M-F-1, National Aperture, inc., Salem, NH) capable of 1D-scanning a distance of 25 mm for side-firing delivery. The motorized stage was connected to a PC via USB connections and operated with Labview software. A 30-cm-long, stainless steel rod (2.7-mm-ID, 3.4-mm-OD, HTX-10R-24-05, Small Parts, inc., Miami Lakes, FL), capable of being inserted through a standard 5-mm-ID laparoscopic port was attached to the stage. This rod housed all of the optics inside a quartz capillary tube (2.0-mm-ID, 2.4-mm-OD, CV2024, Vitrocom, Mountain Lakes, NJ). An aspheric lens (2-mm-OD, 350430-C, Thorlabs, Newton, NJ) for collimation, a 45^{o} rod mirror (2-mm-OD, NT54-091, Edmund Optics, Barrington, NJ) with custom gold coating (International Micro Photonix, inc., Tewksbury, MA) for side-firing delivery, and glass ferrule (Vitrocom, Mountain Lakes, NJ) for centering the optics were glued into place inside a quartz capillary tube (2.0-mm-ID, 2.4-mm-OD, CV2024, Vitrocom, Mountain Lakes, NJ). Figure 2.1 shows photographs of the handheld probe.

Using this custom handheld probe design, two different laser probes capable of providing a Gaussian spatial beam profile with a 200-µm-core low-OH silica/silica multimode optical fiber with 0.22 numerical aperture (NA) and with a single-mode optical fiber (the core diameter of 9 µm, NA of 0.14) were built. Razor blade scans were performed at different working distances from the fiber-lens assembly to measure the laser beam diameter and the degree of beam collimation for both custom probes. Figure 2.2a shows the collimation of the laser beam (λ = 1870 nm), delivered by the multimode optical fiber ONS probe, over a distance of approximately 15 - 30 mm. The probe with

single-mode fiber provides a collimated laser beam at the wavelength of 1455 nm over a distance of approximately 10 - 25 mm (Figure 2.2b). These working distances are sufficient for use in laparoscopic surgery typically performed under high magnification with a camera inserted through a separate laparoscopic port.

The spatial beam profiles at the output end of both probes consisting of a 200-µm-core multimode optical fiber and a 9-µm-core single-mode optical fiber are shown in Figure 2.3ab, respectively. 2D and 3D images for these two Gaussian probes emitting near-infrared laser radiation at the wavelength of 1870 nm (Figure 2.3a) and at the wavelength of 1455 nm (Figure 2.3b) were acquired with an infrared beam analyzer (Pyrocam III, Spiricon, Logan UT).

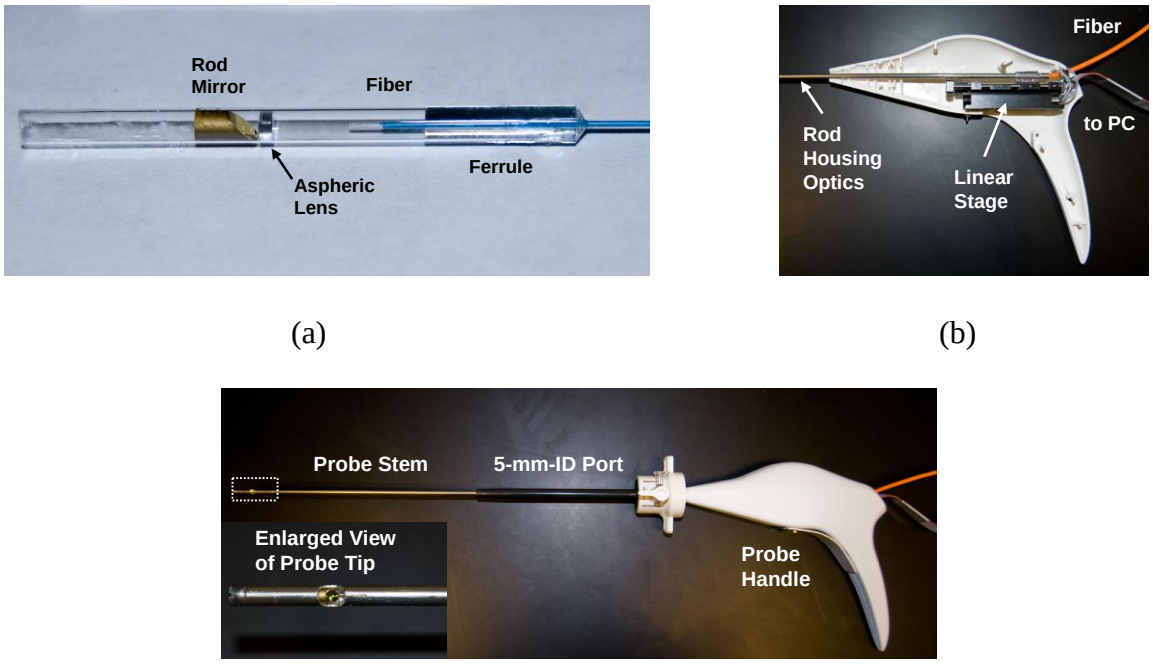

(a) (b)

(c)

Figure 2.1: Probe design: (a) Optical component assembly; (b) Linear stage inside probe handle; (c) Assembled probe.

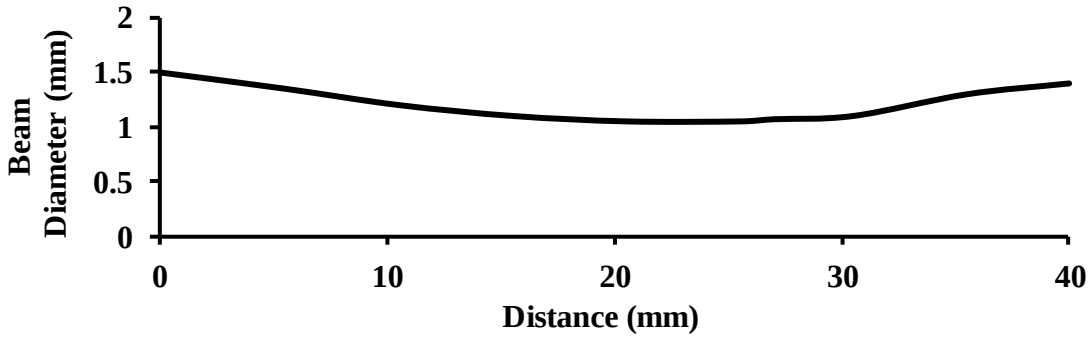

(a)

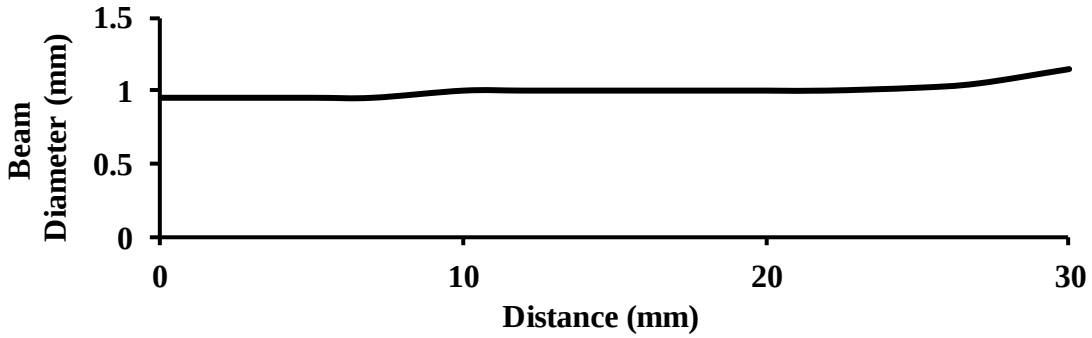

(b)

Figure 2.2: Beam diameter ($1/e^2$) of Gaussian laser beams as a function of working distance for the both probes at the wavelength of (a) 1870 nm and (b) 1455 nm. The spot diameter remains at 1.1 mm diameter (a) and at 1 mm diameter (b) over a distance of approximately 15 mm.

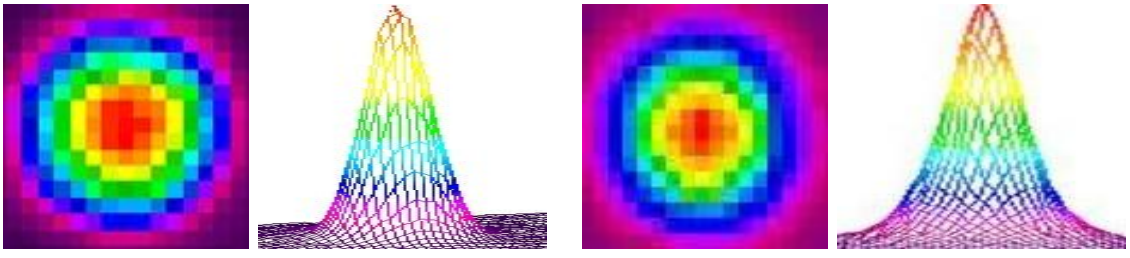

(a) (b)

Figure 2.3: Spatial beam profile images of both probes at wavelengths of (a) 1870 nm and (b) 1455 nm acquired with an infrared beam analyzer in 2D and 3D formats.

2.3 Flat-top Probe Design

Delivery of a flat-top spatial beam profile for the laser beam exiting the fiber optic probe and incident on the nerve surface may be desirable because it provides more uniform irradiation of the nerve and simplifies alignment of the laser beam with the microscopic nerve as well (Figure 2.4ab). With modification, the ONS probe is capable of delivering a collimated 1-mm-diameter, flat-top spatial beam profile to the nerve surface.

Wet chemical etching of the distal fiber tip, producing a concave shape, based in part on a previous report was performed for fiber optic beam shaping to help transform the Gaussian to a flat-top spatial beam profile in these studies [27, 35]. Computer simulations were also performed to optimize the probe design parameters.

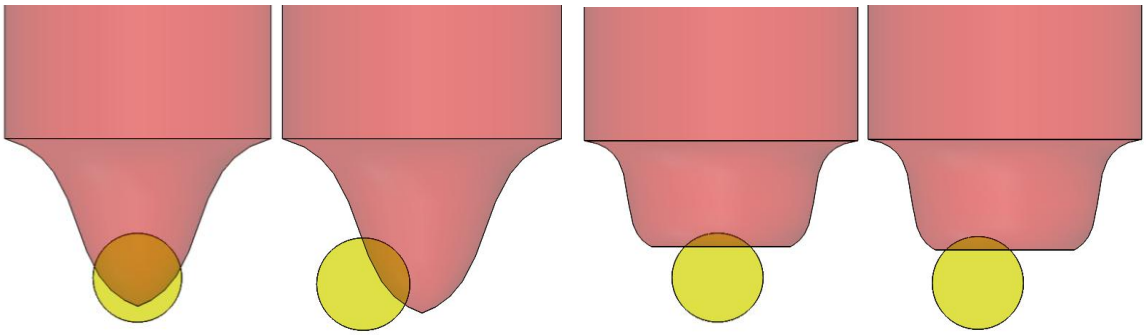

(a) (b)

Figure 2.4: Comparison of (a) Gaussian spatial beam profile and (b) flat-top spatial beam profile on the surface of the nerve for optical stimulation of the CN's in a rat model. Flat-top beam profile provides more uniform nerve irradiation and simplifies alignment of the laser beam.

2.3.1 Fiber Optic Beam Shaping: Chemical Etching

Optical fiber tips can be modified by several different methods, including mechanical drawing, a microprocessing technique, and brittle fracture of the fiber tip [36]. Although these methods are faster, more precise and more reproducible than a chemical etching technique, it is a simple mechanism and a less expensive experimental setup for fabrication of the optical fiber tips.

In this technique, selective etching was employed using the etching speed difference between the core and the cladding of the optical fiber which are formed with doped materials such as germanium (Ge)-doped silica or fluorine (F)-doped silica.

Standard single-mode fiber (9/125 μm, SMF-28+) with a 9-μm Ge-doped silica core, 125-μm pure silica cladding, and 0.14 NA was used in ONS studies with 1455 nm and 1550 nm pigtailed single-mode diode lasers. The fiber tips were carefully cleaved and stripped to a length of 1.5 mm and the core of the distal fiber tip was etched with hydrofluoric (HF) acid (J. T. Baker, Philips) for 90 seconds at room temperature and then the etched fibers were cleaned thoroughly in distilled (DI) water. During the etching process, the fiber was surrounded by 49% HF acid diluted with DI water in the ratio 1:4 (acid/water). A schematic illustration of the experimental setup, used for chemical etching studies of a 9 μm core optical fiber with HF acid, is shown in Figure 2.5.

Figure 2.6 shows the distal fiber tip under magnification after chemical etching of the single-mode fiber. Since the etching speed in the Ge-doped silica core is faster than in pure silica cladding [37], selective chemical etching with creation of a concave cone on the fiber tip is achieved. The spatial beam profile transformation from Gaussian to flat-top profile with a flat-top diameter to spot diameter ratio of 88% was obtained by

forming a concave cone fiber tip with a width of 15 μm and depth of 3.75 μm. The chemical etching rate with HF acid solution was calculated to be 7.36 $\mu m^3/s$ and the NA of the chemically etched fiber tip was measured to be ~ 0.6. A summary of the chemical etching conditions, measured and calculated values is provided in Table 2.1.

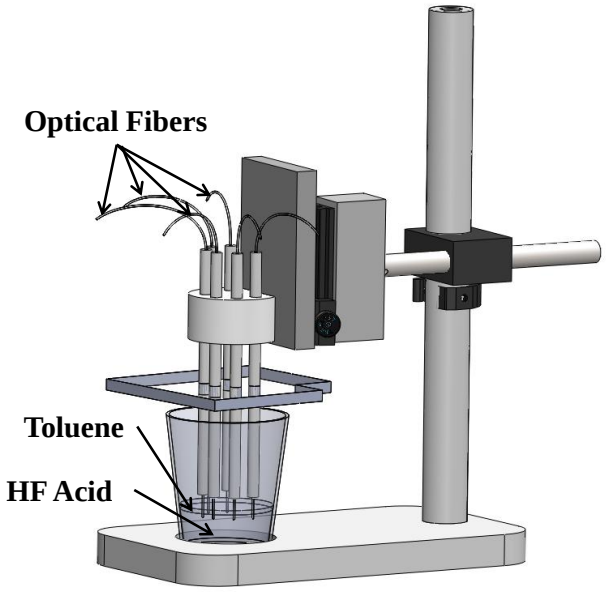

Figure 2.5: Illustration of experimental setup for HF acid etching of optical fibers.

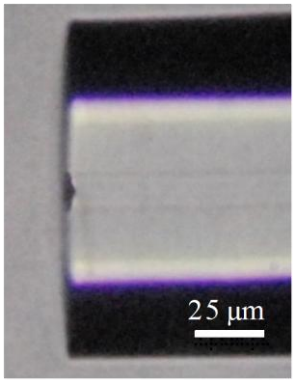

Figure 2.6: Photograph of chemically etched single-mode fiber tip. Etched area measured 3.75 μm depth and 15 μm width for. The etch time was 90 seconds.

Table 2.1: Wet chemical etching conditions and measurements of the concave cone fiber tip of single-mode fiber.

Parameters	Value
HF Acid Solution:	49%
Temperature (^{o}C):	25
Etching Time (s):	90
Width of Cone (μm):	15
Depth of Cone (μm):	3.75
Etching Rate (μm^{3}/s):	7.36
NA:	0.6

2.3.2 Fiber Optic Beam Shaping: Computer Stimulations

Computer simulations using fiber optic ray tracing software (RSoft Photonics CAD Suite Version 8.0.1), based on advanced finite difference beam propagation techniques, were used to assist in optimizing the chemical etching conditions to convert the Gaussian to a flat-top spatial beam profile. These simulation studies also helped to determine the optimal position of the aspheric lens for capturing and collimating the flat-top spatial beam profile.

The computer simulation result in 3D format for the single-mode optical fiber with a core diameter of 9 μm is shown in Figure 2.7. The laser radiation at the wavelength of 1455 nm propagates through the chemically etched distal fiber tip with a Gaussian spatial beam profile, and then is transformed to an approximately flat-top spatial beam profile over a distance of approximately 3.5 mm in free space. The aspheric collimating lens was placed at this distance, to capture and collimate this flat-top beam profile.

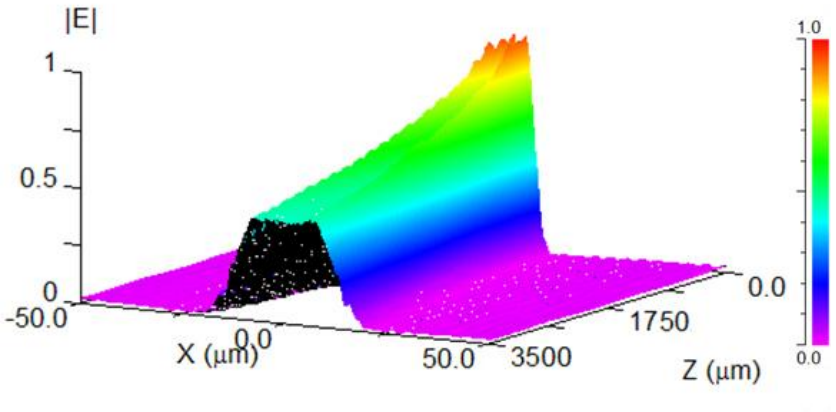

Figure 2.7: Computer simulations show transformation of laser spatial beam profile from the Gaussian mode to approximately flat-top mode in 3D format after the near infrared laser beam propagates through the chemically-etched distal 9 μm core diameter optical fiber tips.

2.3.3 Fiber Optic Beam Shaping: Results

Razor blade scans were performed at different working distances to measure the beam diameter and the degree of beam collimation of the flat-top laser beam through the assembled laparoscopic probes. An approximately 1 mm ($1/e^2$) laser spot diameter and collimation of about 40 mm was obtained for the flat-top probe with a single-mode fiber, as shown in Figure 2.8.

The 2D and 3D images, acquired with an infrared beam analyzer, of the flat-top spatial beam profile for the 1455 nm infrared laser beams are provided in Figure 2.9, after chemical etching of the fiber tip was performed. While further reduction in the wings of the flat-top beam would be ideal, we obtained a relatively flat-top spatial beam profile producing a more uniform intensity distribution on the nerve surface during optical stimulation, thus providing improved alignment and more reliable ONS than the Gaussian spatial beam profile.

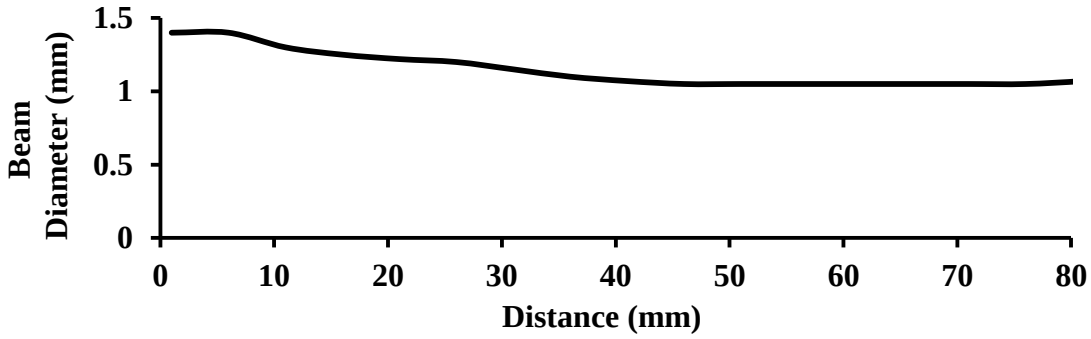

Figure 2.8: Beam diameter as a function of working distance for the flat-top probe with a 9 µm core diameter optical fibers. The beam remains at approximately 1 mm diameter over a distance of 40 - 80 mm.

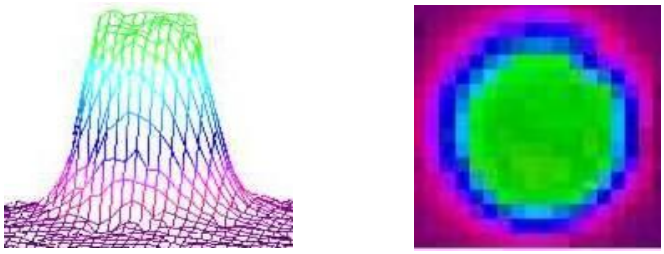

(a) (b)

Figure 2.9: Spatial beam profiles of the flat-top infrared 1455 nm laser beams in (a) 3D and (b) 2D taken with an infrared beam analyzer.

2.4 Conclusions

In summary, three different laparoscopic laser probes consisting of single-mode optical fiber with a core diameter of 9 µm and multimode optical fiber with a core diameter of 200 µm; and capable of providing a collimated, 1-mm-diameter Gaussian and flat-top infrared laser radiations at the wavelength of 1870 nm and 1455nm were designed and assembled for use in optical stimulation of the rat CN. All of these 3-mm-

OD probes are capable of fitting through the smallest standard laparoscopic port (5-mm-ID) currently used in laparoscopic and robotic prostate cancer surgery.

CHAPTER 3: PULSED VERSUS CONTINUOUS-WAVE OPTICAL NERVE STIMULATION

3.1 Introduction

Light can interact with tissue in four ways: transmission, scattering, reflection and absorption. Transmission refers to passing laser light through a tissue without having any effects on the tissue. Reflection refers to reflecting light off the surface of the tissue without any propagation into the tissue. Scattering, diffusion of the laser light within tissue, may become a significant effect after light enters into the tissue. Scattering is a major source of attenuation in biological tissues. Optical absorption by a specific absorber is the fundamental goal of bio-photonic studies in terms of size and shape of inhomogeneities, and refractive index difference between them and tissue. Absorption of laser light in biological soft, homogenous, tissue dominates the attenuation as compared to scattering and originates primarily from water absorption at the infrared wavelengths used during ONS. In general, the amount of laser radiation absorbed in tissue after propagating over a path length x may be computed by an exponential decay equation 3.1;

$$I = I_o e^{-\mu_a x} \tag{3.1}$$

where I_o is initial intensity (J/cm^2), I is final intensity (J/cm^2) at distance x (cm) and μ_a is an absorption coefficient (cm^{-1}). The Beer-Lambert Law of absorption states that the intensity of light exiting from an optical absorption layer in soft tissue is exponentially related to the intensity entering the soft tissue.

The sequence of events in photon interaction with tissue may be summarized based on the following: laser radiation is absorbed by the target absorber, water, the primary source of optical absorption in soft tissues in the infrared spectrum. Several possible effects may occur in the tissue, including photochemical, photomechanical and photothermal [38-40].

In a photochemical interaction, if the individual photon energy is large enough as it may be in the ultraviolet (UV) spectrum, molecular bonds are directly broken [41]. This depends on the photon energy having a perfect match with the bond energy of the target molecule. Since infrared wavelengths with enough tissue absorption of laser radiation can trigger neural stimulation, we can conclude that the mechanism for ONS may not be a result of photochemical effects from laser-tissue interaction.

In a photomechanical interaction, a high power density above ~ 1 kW/cm^2 with very short pulses (in nanosecond scale or less) makes mechanical side effects more significant during laser-tissue interaction [39]. The photomechanical interaction with tissue produces shock wave generation and jet formation, resulting in localized mechanical rupture. Since the laser is operated at very low pulse energy with long pulse durations on the scale of milliseconds or even CW for successful ONS, a photomechanical process is also not the primary mechanism.

Some research groups have recently arrived at the hypothesis that the mechanism of ONS is mainly related to photothermal effects resulting from the transformation of absorbed optical energy into heat [42-44]. However, the details of this mechanism responsible for ONS are still not yet fully understood. Thus, it is critical to build up a

basic idea about the interaction between infrared laser radiation and tissue during optical nerve stimulation.

Furthermore, light and tissue interaction is the combined effect of the properties of the laser radiation and the optical properties of the tissue. ONS, a novel method of stimulation of neural tissue, in vivo, is an example of interaction of infrared light with soft tissue, mainly mediated by a thermal process, and depending on the operational parameters of the laser. These laser stimulation parameters introduce a large matrix of variables that need to be optimized for consistent and reliable nerve stimulation. One of the key parameters of this interaction is wavelength. It determines optical penetration depth (OPD) and distribution in soft tissue. For the majority of IR laser wavelengths used in ONS, absorption of optical energy (as opposed to scattering) is the dominant factor in attenuation (Figure 3.1). Another major parameter is the pulse repetition rate of the laser. It determines how fast the required total amount of energy is deposited into the nerve for initiating neural activity.

Very few studies have been reported on optimization of the optical parameters in ONS [14, 45-46]. In addition, parameters that were optimized for several applications, including motor nerve and cochlea nerve stimulation, are not necessarily the ideal parameters to be used for stimulation of the rat CN.

Therefore, Chapter 3 describes experimental setups including animal studies, describes optical stimulation of the rat CN in terms of intracavernous pressure (ICP) responses by comparing Thulium fiber laser operation in pulsed mode with variable repetition rates and in CW mode, respectively, and also explores the effect of the laser

parameters on nerve temperature in order to gain further insight into the biophysical mechanism underlying the phenomenon of ONS by IR laser radiation.

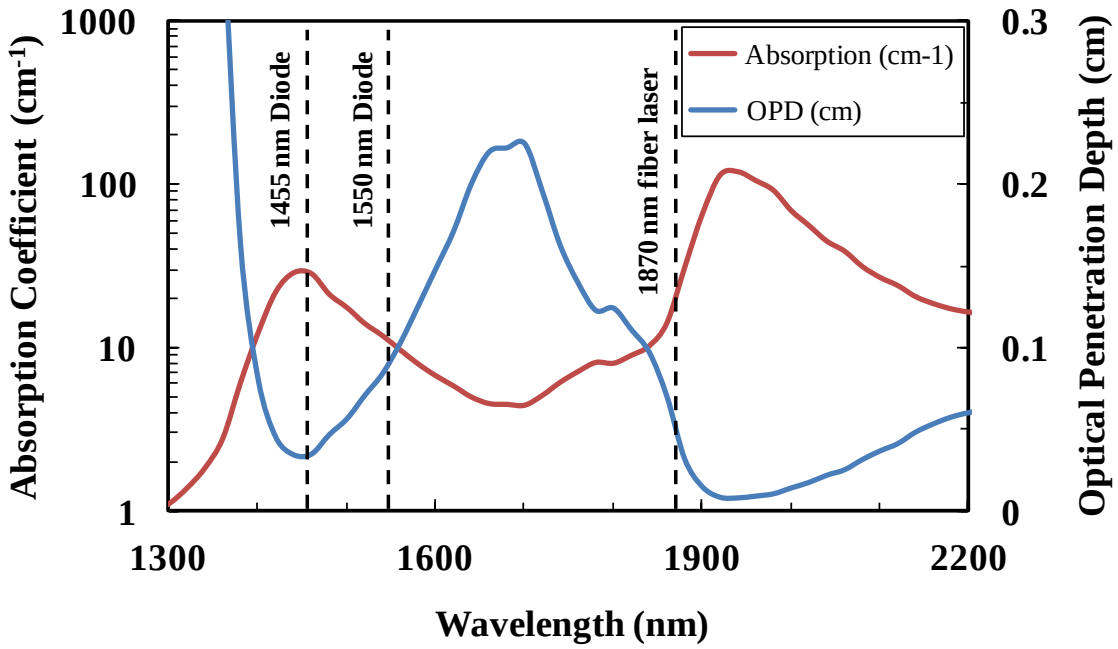

Figure 3.1: The absorption coefficient (red line) and optical penetration depth (blue line) of infrared laser radiation in water (the dominant absorber in soft tissue) as a function of wavelength. The wavelengths of the Thulium fiber laser and infrared laser diodes used in our ONS studies are labeled.

3.2 Materials and Methods

All animal studies were performed in rats, in vivo, in the Neurourology laboratory at Johns Hopkins Hospital (Baltimore, MD). Sprague Dawley rats weighing 400 - 600 grams were used in these studies. Care and use of the animals in this study were performed under an approved animal protocol. At the completion of the study, the rats were euthanized by intracardiac injection of potassium chloride while under anesthesia,

as is consistent with the recommendations of the Panel of Euthanasia of the American Veterinary Medical Association.

The rats were anesthetized by intraperitoneal injection with 50 mg/kg sodium pentobarbital. They were secured in the supine position and prepped for surgery. The CN arising from the ipsilateral major pelvic ganglion situated dorsolateral to the prostate was exposed via a midline suprapubic incision and anterior pelvic dissection. An increase in ICP in the rat penis after optical stimulation was measured by a 23-G needle placed in the base of the penis and connected to tubing that ran to a transducer (Harvard Apparatus, Holliston, MA) and data acquisition system (DI-190; DataQ Instruments, Akron, OH). MATLAB software was used to analyze the corresponding response data. Figure 3.2 shows a photograph of the rat surgical preparation.

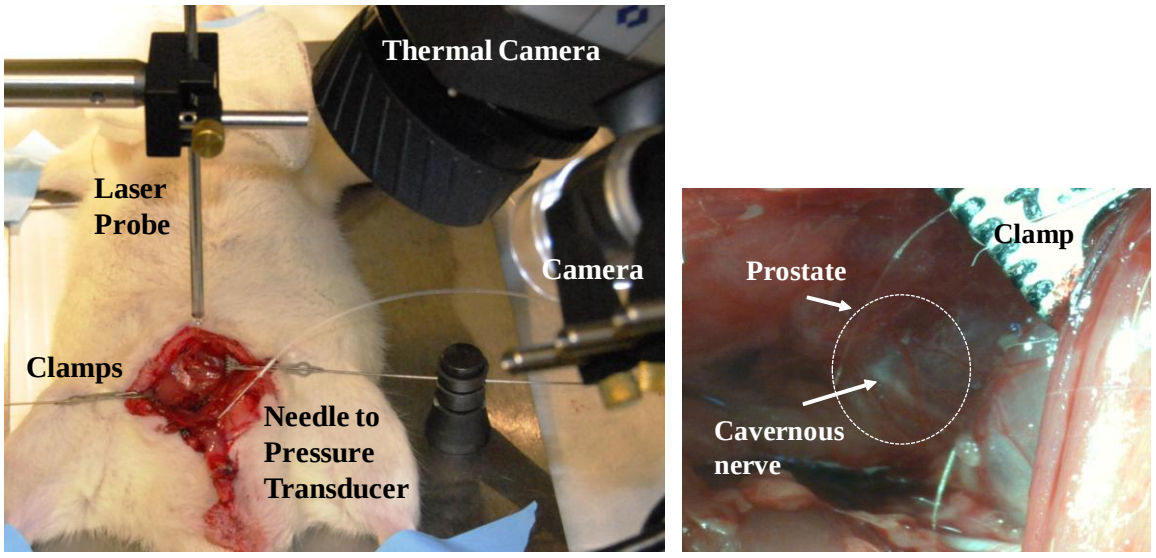

(a) (b)

Figure 3.2: Photograph of surgical preparation of rat for ONS and temperature measurements: (a) Complete setup; (b) Close-up view of the cavernous nerve on the surface of prostate.

Pulsed versus CW laser radiation optical stimulation of the rat CN studies were conducted with a 5.5-Watt Thulium fiber laser (TLT-5, IPG Photonics, Oxford, MA) operated at 1870 nm. Figures 3.3 and 3.4 show a photograph of the fiber laser and a diagram of the experimental setup, respectively.

Figure 3.3: Compact, portable, and tunable wavelength of 1850 nm to 1880 nm Thulium fiber laser was used in the nerve stimulation studies.

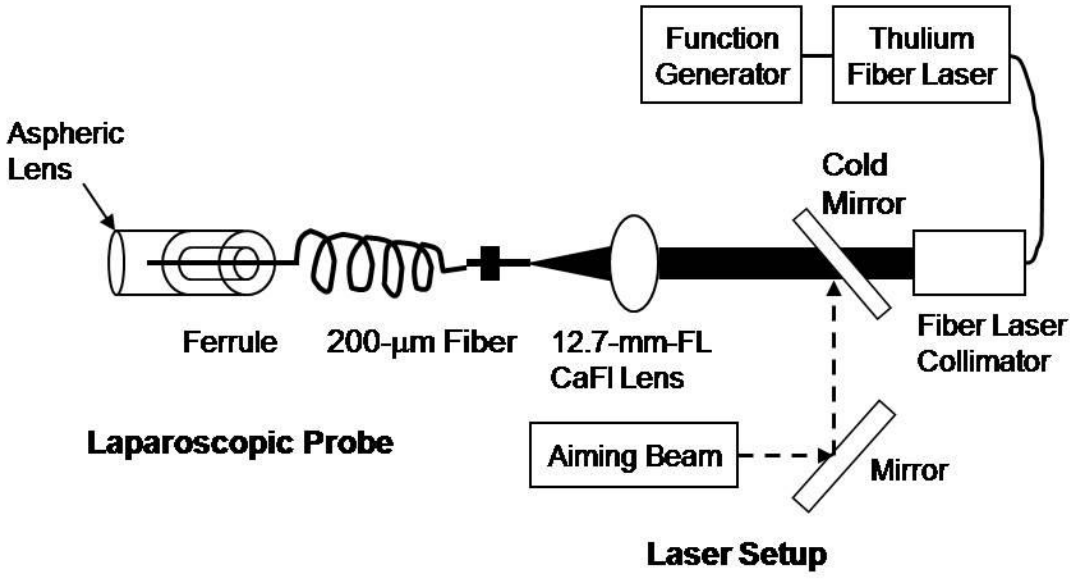

Figure 3.4: Diagram of experimental setup with fiber optic assembly for the laparoscopic laser probe (left) and laser equipment (right).

Most soft tissues are approximately 70 - 80% water which is the primary absorber in the IR spectrum. The water absorption curve shown in Figure 3.1 thus provides a good approximation of the wavelength needed to closely match the optical penetration depth (OPD) of about 400 µm to the diameter of the rat CN's for reliable and consistent ONS. Figure 3.5 shows a photograph of a dissected rat CN, measuring 300 - 400 µm in diameter.

Figure 3.5: Photograph of dissected rat CN, measuring 300 - 400 µm in diameter.

The fiber laser was operated in either CW mode, or in pulsed mode with 5 ms pulse duration at 10, 20, 30, 40, 50, and 100 Hz. The laser pulse duration of 5 ms was chosen, based on previous reports that have shown that the threshold radiant exposure for ONS is relatively independent of pulse duration in the range of 5 µs - 5 ms [42]. The IR laser radiation was coupled into a laparoscopic probe, capable of providing a 1.1-mm diameter (corresponding to an area of 0.0095 cm^2) collimated quasi-Gaussian laser beam with a 200 µm-core-diameter optical fiber, as previously described in Chapter 2.

The probe tip was positioned approximately 15 mm above the nerve on the surface of the rat prostate, as shown in Figure 3.2a. A digital microscope with variable magnification (AD413TL Dino-lite, Torrance, CA) was focused onto the prostate surface to improve alignment of the laser beam with the nerve surface. A thermal camera (A20M, Flir System, Boston, MA) provided real-time temperature mapping of the rat CN surface during optical stimulation to optimize the laser stimulation threshold parameters, to identify the threshold for thermal damage, and to gain further insight into the laser-tissue interaction mechanism of ONS.

Two laser parameters were varied for this study, the laser pulse repetition rate (10 - 100 Hz, CW) and the laser pulse energy (0.28 - 6.37 mJ), which corresponded to a radiant exposure of 0.03 - 0.67 J/cm^2 for the fixed laser spot diameter of 1.1 mm. The laser pulse energy was escalated in small increments until the radiant exposure reached the threshold for ONS. The ICP response was then measured at or just above the stimulation threshold, providing safe and reproducible stimulation while preventing undesirable thermal damage to the nerve.

3.3 Results

Figure 3.6 shows the threshold pulse energy (mJ) for ONS as a function of repetition rate (Hz). As the pulse rate is increased during the stimulation time of 15 s, the minimum pulse energy needed to initiate nerve stimulation decreases significantly. In other words, the required optical energy to create the desired photothermal effect in the nerve for stimulation is achieved at a high pulse repetition rate with lower pulse energy.

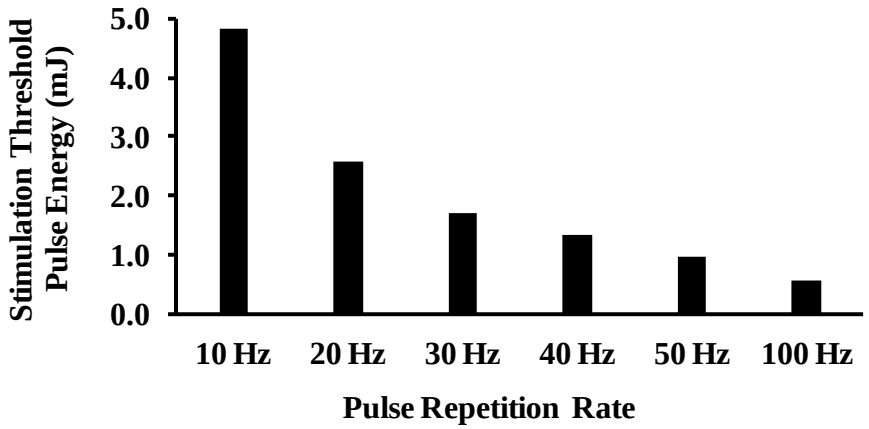

Figure 3.6: The pulse energy threshold decreased significantly as a function of the pulse repetition rate.

In the second part of these studies, the Thulium fiber laser was operated in CW mode with exactly the same experimental set-up and stimulation time (15 s). Figure 3.7 shows a representative example of ICP response of the CN as a function of time to CW IR laser stimulation for 15 s duration at a total energy threshold of around 0.71 J. ONS at the threshold energy level produced a strong response in the rat penis with the ICP increasing from a baseline of 16 mm Hg to a peak of 39 mm Hg. The time delay between the beginning of the stimulation and ICP response at the threshold level was measured to be nearly 10 s, closely corresponding to the time necessary for the CN's to heat up above a threshold temperature measured to be ~ 43 ^{o}C.

As expected, deposition of sufficient thermal energy in the nerve for successful and repeatable nerve stimulation may be expedited by increasing the pulse repetition rate accordingly. Since total energy needed to give a start to stimulation was provided in a shorter time by increasing the pulse rate of the laser and at the end operating in CW mode, a faster ICP response was obtained during the 15 s ONS, shown in Figure 3.8. The

ICP response time decreases from the longest time delay of ~ 17 s at 10 Hz to the shortest time delay of ~ 10 s at CW corresponding to how fast the photothermal effect is achieved in the nerve.

Thermal effects on the surface of the CN were quantified in a rat model, in vivo, with the use of a thermal camera to accurately define the stimulation threshold in terms of the required minimum amount of energy to have a photothermal effect for reliable and consistent ONS. The baseline temperature of the nerve surface just prior to stimulation, the maximum temperature immediately after ONS, and temperature changes during the stimulation were recorded in these studies. Figure 3.9 shows representative thermal images of the rat CN before ONS and at peak temperature during the stimulation, for the same stimulation parameters and results as shown in Figure 3.7. It should be noted that the baseline nerve temperature was not at normal body temperature (around 37 ^{o}C), but rather a few degrees cooler (~ 34 ^{o}C), due to the open surgical model used in these studies (Figure 3.2a).

Table 3.1 provides a comprehensive summary of the results for the temperature and CW versus pulsed ONS studies. The stimulation threshold pulse energy, radiant exposure, average power, total energy, and temperature for successful ONS are reported, along with the ICP response time. The pulse energy and threshold radiant exposure for successful ONS were not fixed as previously thought, but rather decreased significantly as the laser pulse rate was increased. The stimulation threshold, however, was not dependent on average power delivered to the nerve. Although there was some variation in the results, the ICP response time continued to decrease as the pulse rate was increased, with CW irradiation providing the fastest ICP response time. It should be noted that for

the 10 Hz data set, the delayed ICP response actually occurred just after the end of the 15 s laser irradiation time. Finally, experimental data have shown that the absolute temperature threshold for nerve stimulation was measured to be 42 to 45 ^{o}C. Results presented here suggest that sodium gates, initiating a depolarization to create an action potential series, are opened at a certain temperature level. As the temperature is increased further, the amplitude and duration of the train of action potentials increase accordingly, providing higher and faster ICP responses [23].

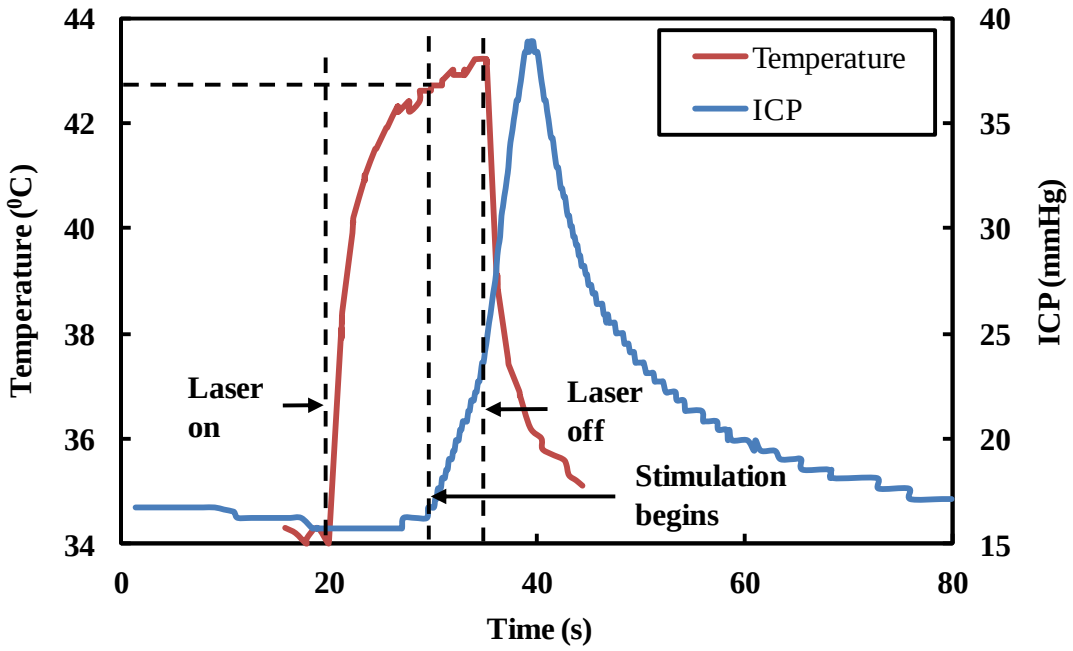

Figure 3.7: Continuous-wave optical stimulation of the rat cavernous nerves (CN's). Wavelength = 1870 nm, spot = 1.1 mm, power = 47 mW, total energy = 0.71 J, and stimulation time = 15 s. A delayed response is observed in which the intracavernous pressure (ICP) response in the rat penis begins to increase approximately 10 s after laser irradiation begins (at t = 20 s) and then continues to increase after laser irradiation ends (at t = 35 s). Note that the surface of the CN reaches a stimulation threshold temperature of approximately 43 ^{o}C after 10 s of laser irradiation (at t = 30 s), closely corresponding to the onset of the increase in ICP.

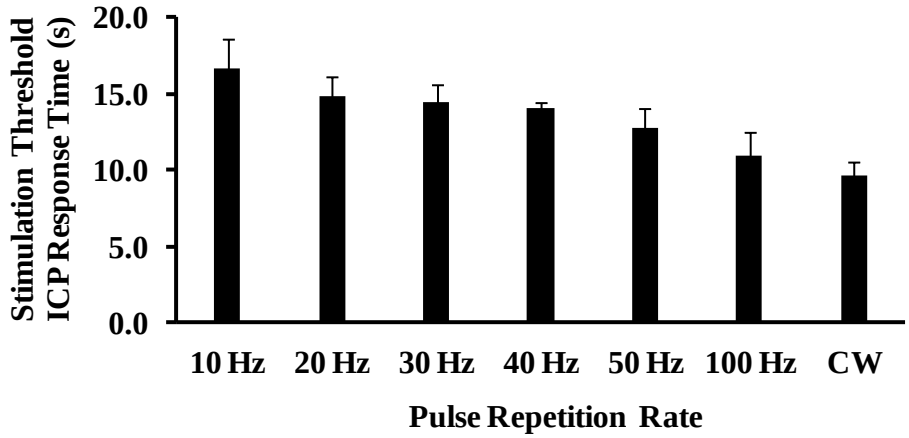

Figure 3.8: The ICP response times at the stimulation threshold levels as a function of repetition rate and CW mode.

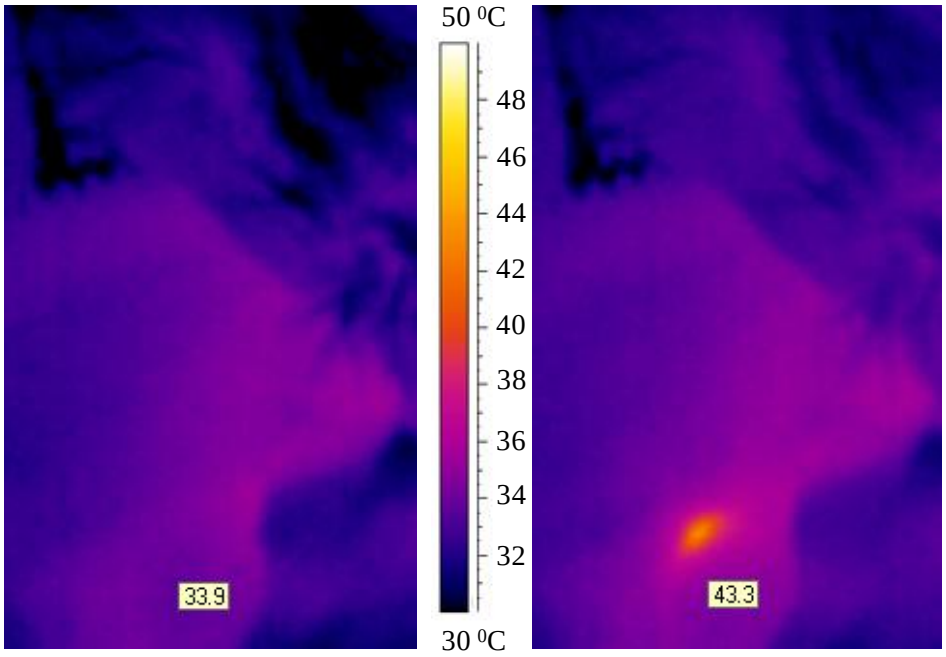

Figure 3.9: Thermal images of the CN: (a) Temperature of the nerve just before laser irradiation was at a baseline level of 33.9 ^{o}C; (b) The nerve reached a peak temperature of 43.3 ^{o}C during laser irradiation, which was just above the nerve stimulation threshold. The orange region showing the peak temperature in the thermal image on the right is approximately the same size as the 1.1 mm diameter laser spot used for heating the cavernous nerve (which has a diameter of 200 - 400 μm).

Table 3.1: Optical nerve stimulation threshold parameters for continuous-wave versus pulsed laser radiation for a 15 s duration.

	Laser Pulse Repetition Rate						
Parameters	**10 Hz**	**20 Hz**	**30 Hz**	**40 Hz**	**50 Hz**	**100 Hz**	**CW**
Pulse Energy (mJ):	4.84	2.57	1.71	1.34	0.94	0.56	NA
Incident Fluense (J/cm^2):	0.51	0.27	0.18	0.14	0.1	0.06	NA
Average Power (mW):	48.4	51.3	51.2	53.6	47.2	55.5	47.3
ICP Response Time (s):	16.7±1.9	14.8±1.3	14.5±1.1	14.0±0.5	12.8±1.3	10.9±1.6	9.7±0.8
Total Energy until Stim. (J):	0.73	0.76	0.74	0.75	0.6	0.6	0.46
Temperature (^oC):	43.8±1.3	42.3±1.1	42.3±0.2	41.5±0.6	44.9±1.2	44.7±1.2	42.9±0.3

*NA= Not applicable

*CW=Continuous-wave

*ICP=Intracavernous pressure

3.4 Discussion and Conclusion

Experimental results reported in this chapter show that neural activity and optical energy deposited into the tissue are directly related to each other in terms of stimulation threshold and ICP response time. These results also imply that there may be a threshold tissue temperature that must be reached by delivering sufficient total optical energy to create a required photothermal effect and generate nerve stimulation.

Operation of a Thulium fiber laser in CW mode results in a faster deposition of the laser energy into the nerve and a faster ICP response time for short-term ONS. This observation may be important in intra-operative diagnostic applications requiring rapid feedback, such as identification and preservation of the cavernous nerves, which are responsible for erectile function, during prostate cancer surgery.

The results of this study also further confirm that ONS operates primarily based on a photothermal mechanism [42], in which light energy is converted to heat energy in

the nerve, until a sufficient amount of heat is generated to increase the nerve temperature above a threshold value (42 - 45 ^{o}C) for activation of neural activity. In addition, a strong correlation was observed between the laser irradiation time necessary to raise the nerve temperature above the stimulation threshold and the onset of ICP response.

In summary, a Thulium fiber laser with a probe providing a collimated quasi-Gaussian laser beam was operated in CW mode and successfully produced faster ICP response time in the optical CN stimulation in a rat model, in vivo, than did pulsed laser irradiation. This result allows the development of a much less expensive and more compact ONS system for further optical nerves stimulation studies and for potential diagnostic applications, to be described next in Chapter 4.

CHAPTER 4: ALL-SINGLE-MODE FIBER DESIGN FOR CONTINUOUS-WAVE INFRARED OPTICAL NERVE STIMULATION

4.1 Introduction

Successful optical stimulation of the rat cavernous nerves using both pulsed [19-20, 23] and continuous-wave (CW) [24] infrared laser radiation has been previously reported in Chapter 3. CW infrared laser irradiation during optical stimulation of neural tissue has been shown to result in faster deposition of energy into the nerve, thus producing a more rapid ICP response in the rat penis. This approach may also allow the use of a less expensive and more compact laser system for potential diagnostic applications. In all of our previous studies, the experimental setup utilized a relatively expensive Thulium fiber laser, a complex configuration of bulk optical components, and a multimode fiber optic delivery system (Figure 3.3 and 3.4). This experimental setup introduced a number of limitations, including: (i) high cost optical components, (ii) periodic maintenance for optical alignment and cleaning, and (iii) a larger and more expensive ONS system.

In this chapter, we utilize an inexpensive and compact pigtailed single-mode diode laser, an all-single-mode fiber (SMF) system design, and fiber optic beam shaping methods for ONS in a rat CN model, in vivo. The results described here define a therapeutic window for safe, reliable, and reproducible short-term optical stimulation of

the CN, which may lead to the development of an intra-operative diagnostic system for identification and preservation of the prostate nerves, which are responsible for erectile function, during prostate cancer surgery.

4.2 Methods and Technology

All measurements were conducted in the Neurourology laboratory at Johns Hopkins Hospital using a total of 14 adult Sprague Dawley rats weighting 400 - 600 grams. Animal preparation and surgery were similarly performed as described previously in Chapter 3 (Figure 3.2).

A pigtailed single-mode infrared diode laser (QFLD-1450, Qphotonics LLC, Ann Arbor, MI) emitting up to 150 mW of power at a center wavelength of 1455 nm (Figure 4.1) was used for ONS of the rat CN.

The laser radiation at this wavelength has an OPD of around 350 μm in water (the dominant absorber in soft tissues in the near- to mid-infrared spectrum) [8], which closely matches the diameter of the rat CN (300 - 400 μm) for uniform irradiation during ONS (Figures 3.1 and 3.5).

This 1455 nm diode laser also represents a more compact and less expensive alternative to the 1870 nm Thulium fiber laser used during our previous ONS studies (Chapter 3), but with an approximately similar OPD.

It should be noted that successful ONS at the wavelength of 1450 nm has been recently reported using a high power pulsed diode laser [47], but not with a low power single-mode diode laser operated in CW mode, as demonstrated in this study.

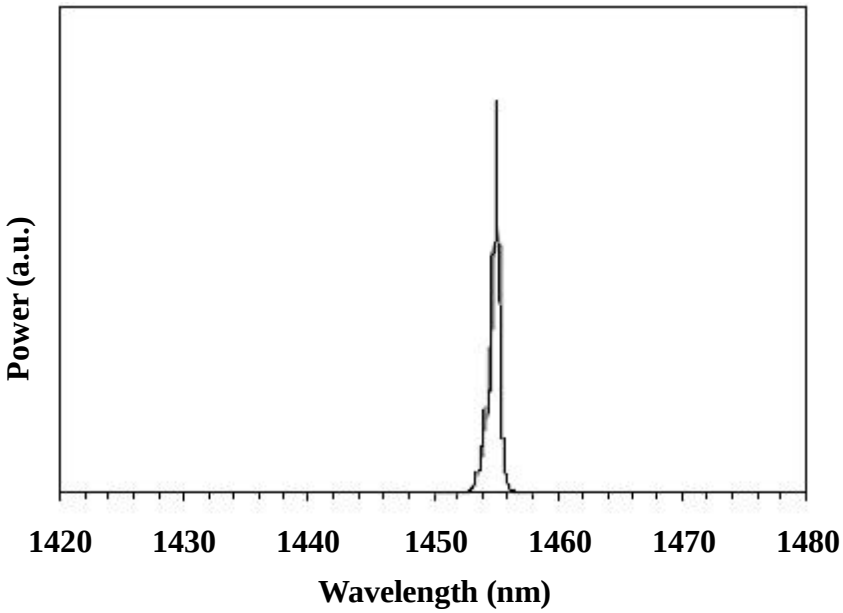

Figure 4.1: The emission spectrum of a pigtailed single-mode infrared diode laser operating at a center wavelength of 1455 nm with a spectral width of 1 nm.

A visible red diode laser (QFLD-660, QPhotonics, L.L.C., Ann Arbor, MI) with a power of 20 mW and a wavelength of 660 nm was coupled into a SMF and used as an aiming beam to provide alignment. A SMF coupler (1x2 SM Dual Window Coupler, Fiber Instrument Sales, Oriskany, NY) with a 10/90 coupling ratio was used for combining both the visible and infrared laser beams into a single SMF for delivery. An optical shutter (SH-200-1480-9/125, Oz Optics, Ottawa, Canada) in the infrared laser SMF arm provided rapid on/off switching of the laser beam during ONS. The output of the fiber coupler was then connected to a custom-built probe consisting of standard SMF (9/125 μm, smf-28+, Corning Optical Fiber, Corning, NY) with an aspheric lens attached to the distal tip for beam collimation. All connections between standard single-mode optical fibers were achieved with FC/APC connectors to prevent back-reflections. Figure 4.2 provides a diagram of the experimental setup and details of the optical components.

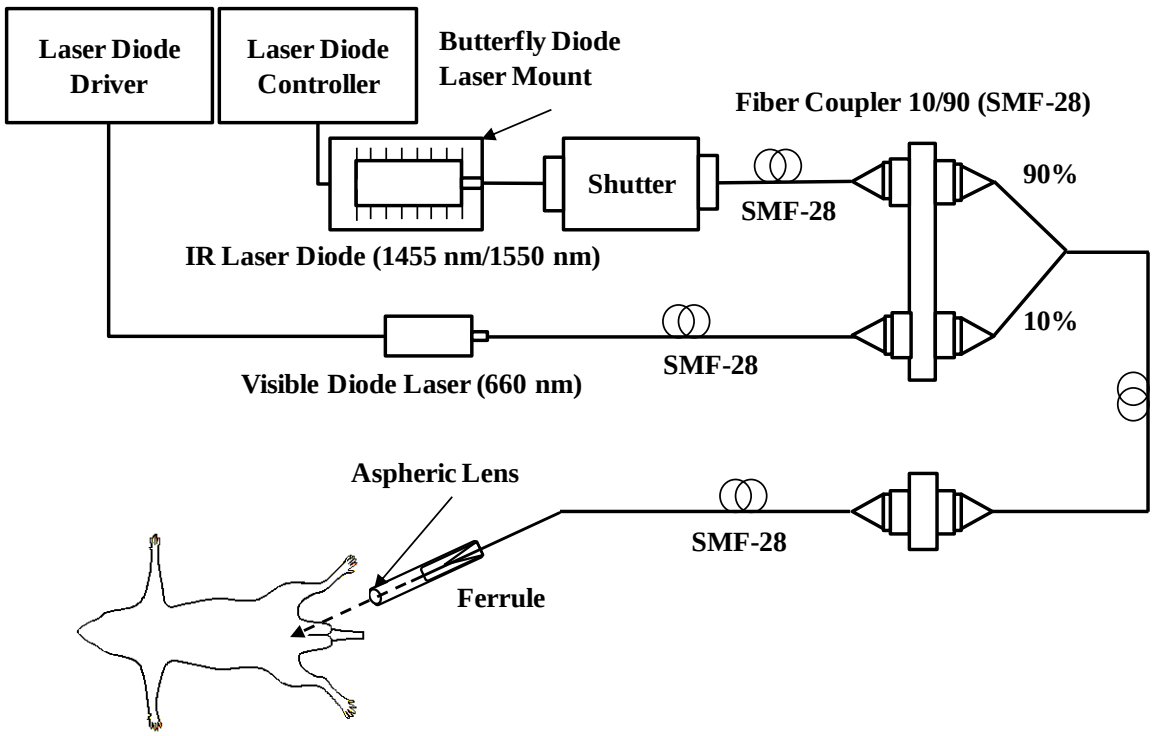

Figure 4.2: Diagram of experimental setup with single mode fiber optic assembly for probe, fiber couple with ratio of 10/90 and laser diodes.

Two different custom-built probes were used in the study explained in this chapter. The probe with a chemically etched SMF provided a collimated, 1-mm diameter, flat-top laser beam profile over a working distance of approximately 40 mm. The other probe with standard SMF was capable of producing a 1-mm diameter, Gaussian laser beam profile with a collimation of about 15 mm. Probe design, assembly and characterization have been previously explained in detail in Chapter 2.

4.3 Results

A summary of the ONS results comparing both the Gaussian and flat-top fiber optic probes is provided in Table 4.1. Each value represents the mean of at least 20 independent measurements ± standard deviation. Rapid ICP response times averaging 4 - 5 s were recorded using both Gaussian and flat-top probes. This rapid ICP response is

critical for intra-operative identification and preservation of the CN during potential diagnostic ONS applications. Near the optical stimulation threshold, comparable ICP response times of approximately 13 s were also observed. These ICP response times represent a significant improvement compared to previous studies which required up to 60 s of stimulation [20]. The minimum incident power needed to stimulate the CN was about 30 mW corresponding to an irradiance of 4 W/cm^2 for the 1-mm-diameter spot size used in these studies.

Successful optical stimulation of the rat CN was achieved at nerve temperatures of around 41 ^oC. There was an upper temperature limit of about 48 ^oC corresponding to an incident power of ~ 55 mW and an irradiance of 7 W/cm^2 at which thermal damage to the nerve was observed. Such nerve damage was noted by both visual observation of the nerve surface under magnification as well as a notable decay in both the ICP response time and magnitude upon repeated stimulations.

Figure 4.3 shows representative ICP responses obtained in the rat penis using both Gaussian and flat-top fiber optic probes when the rat CN was irradiated with a laser power significantly above the stimulation threshold but below the thermal damage threshold for a period of 15 s. ICP increased from a baseline of 5 - 10 mmHg to a peak of approximately 50 mmHg during ONS. This strong ICP response was initiated about 3 - 4 s after laser irradiation began, corresponding to the time necessary to elevate the CN temperature above a threshold temperature of ~ 42 ^oC for these experiments. The maximum temperature on the CN surface was measured to be about 45 ^oC at the end of stimulation, significantly below the damage threshold temperature of 48 - 49 ^oC, previously observed.

Table 4.1: Comparison of threshold and damage parameters for Gaussian and flat-top beam profiles in optical stimulation of rat CN studies.

Parameter	Gaussian	Flat-top
Fastest ICP response time (s):	3.8 ± 0.5	4.8 ± 0.9
Threshold ICP response time (s):	12.7 ± 1.0	13.0 ± 0.9
Power to stimulate (mW):	28.3 ± 5.2	33.8 ± 2.5
Irradiance to stimulate (W/cm^2):	3.6 ± 0.7	3.9 ± 0.3
Temperature to stimulate (^{o}C):	41.3 ± 1.3	41.2 ± 0.6
Power to damage nerve (mW):	55.0 ± 7.5	
Irradiance to damage nerve (W/cm^2):	7.0 ± 1.0	
Total Energy to damage nerve (J):	0.83 ± 0.11	
Temperature to damage nerve (^{o}C):	48.5 ± 1.1	

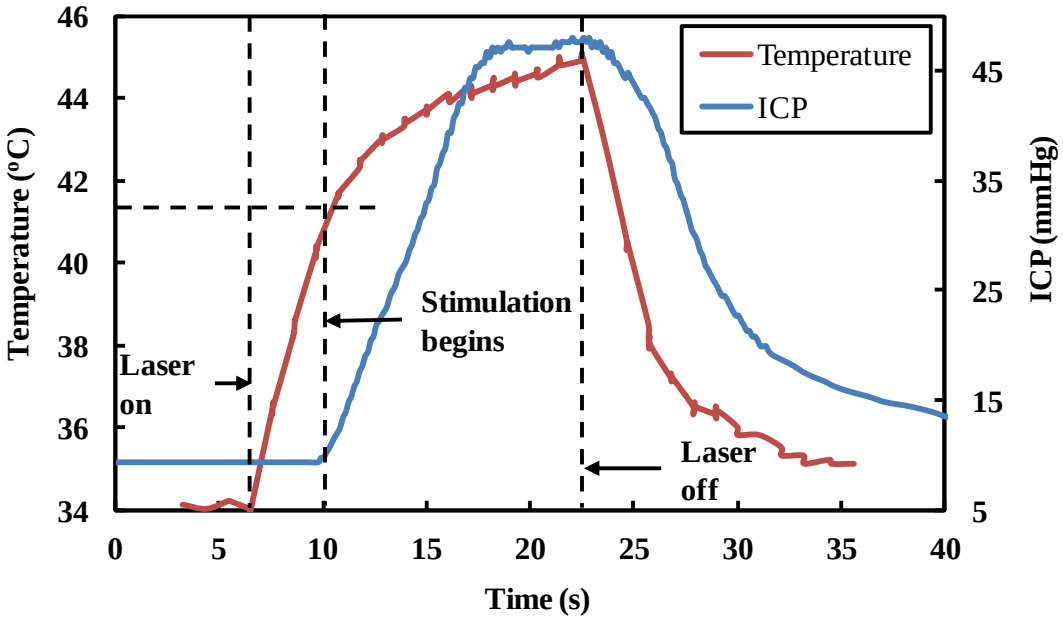

(a)

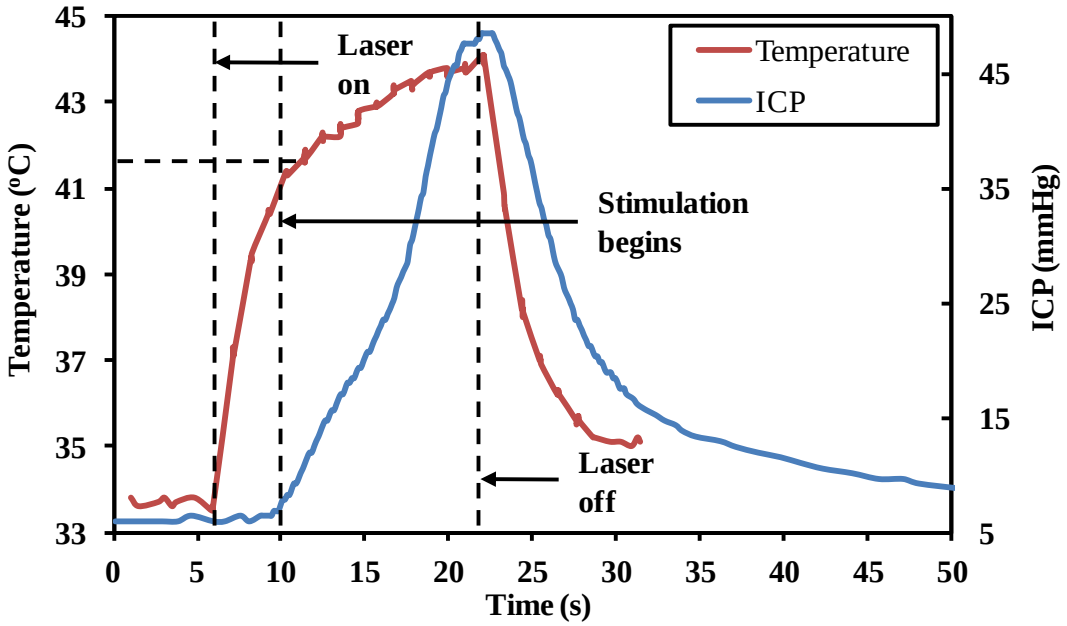

(b)

Figure 4.3: (a) Intracavernous pressure (ICP) response as a function of time for optical stimulation of the rat CN with a Gaussian spatial beam profile (wavelength = 1455 nm, spot diameter = 1 mm, power = 50 mW, total energy = 0.75 J, and stimulation time = 15 s); (b) ICP response as a function of time for optical stimulation of the rat CN with a flat-top spatial beam profile (wavelength = 1455 nm, spot diameter = 1 mm, power = 51 mW, total energy = 0.77 J, and stimulation time = 15 s).

It should be noted that the shape and magnitude of the ICP response curve varies significantly among rats, and is dependent on many anatomical and physiological parameters (e.g. nerve dimensions, blood pressure, etc...) beyond the control of the ONS parameters. Nevertheless, for the purposes of our study, any ICP response measured during ONS which is significantly above the baseline (noise level) may serve as a reliable indicator for positive identification of the CN during prostate cancer surgery. Thus, the ICP signal-to-noise ratio (SNR) of 5:1 (50 mmHg signal / 10 mmHg baseline) shown here provides a sufficient and robust response.

Photographs of the rat CN taken with a digital microscope before and after optical stimulation are provided in Figure 4.4. The surface temperature of the CN reached the maximum value of ~ 48 ^{o}C during 15 s stimulation duration. Visible thermal damage was observed on the nerve surface as shown in Figure 4.4b. The results shown here define an upper limit in temperature for safe ONS of the rat CN with CW infrared laser radiation.

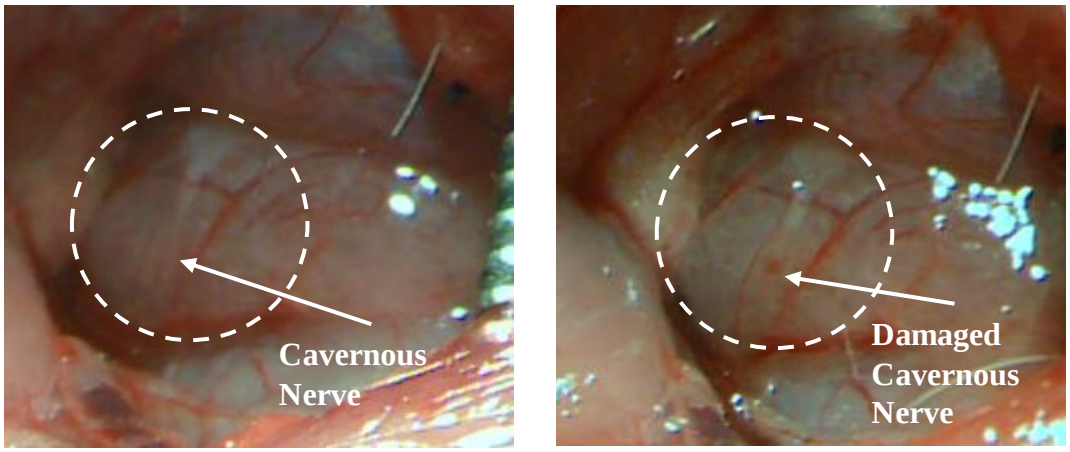

(a) (b)

Figure 4.4: (a) Photographs of the healthy cavernous nerve before ONS and (b) visible thermal damage after ONS as a result of laser irradiation of the nerve (wavelength = 1455 nm, spot diameter = 1 mm, power = 60 mW, total energy = 0.9 J, and stimulation time = 15 s). The peak tissue temperature reached during ONS was approximately 48 ^{o}C.

4.4 Discussion

Optical nerve stimulation using infrared laser radiation has been previously studied as a potential alternative to electrical nerve stimulation. However, the use of quite bulky optical components and high cost infrared lasers (e.g., 20 W Holmium:YAG laser used in urology costs between $30k and $50k and 5 W tunable thulium fiber laser costs $15 to $20k) in some of these studies may represent a significant hurdle for translation of

ONS into the clinical applications. The use of diode lasers with multimode spatial beam profiles coupled to multimode optical fibers for delivery of the laser radiation during ONS may also introduce unnecessary irregularities in the laser beam intensity and difficulty in alignment of the laser beam with the nerve, potentially compromising the safety and consistency of ONS.

Results presented in this chapter demonstrate that a novel all-single-mode-fiber design approach can be used with a low power 150 mW single-mode fiber coupled diode laser (costing approximately $850) for reproducible, safe and short-term CW optical stimulation of the prostate cavernous nerves. These results also further confirm that the minimum required nerve temperature to be reached for initiating nerve activation is about 41 ^{o}C and that visible thermal damage to the nerve is not observed until a temperature of 48 - 49 ^{o}C, as previously reported [31].

It should be noted that ONS with this new SMF configuration demonstrated in the study provides several advantages compared with previous multi-mode fiber optic ONS systems. First, the concept of the new design for ONS eliminates the packing complexities caused with integration of bulk optical components and fiber optics. Second, it reduces the maintenance and manufacturing costs of the ONS system (The entire ONS system may cost less than $5k). Third, delivery of the laser beam through chemically etched single mode optical fiber provides an improved spatial beam profile such as a flat-top beam profile to obtain a uniform intensity distribution across the surface of the nerve.

Although the results in Table 4.1 demonstrate that there is not a significant difference between the Gaussian and flat-top fiber optic probes in terms of the ONS

operating parameters, the flat-top probe allowed simplified alignment of the laser beam with the microscopic nerve, thus providing a more uniform irradiance of the nerve surface and potentially avoiding thermal damage to the nerve from hotspots in the laser spatial beam profile, as mentioned in Chapter 2. This feature may prove critical in other applications where the nerve and laser spot diameter are even smaller and more difficult to co-align.

Finally, analysis of thermal damage to the nerve after ONS was based on a reduction in nerve function (e.g. decay in ICP response time and magnitude) and visible observation of thermal damage to the nerve surface in this chapter. In Chapter 6, investigation of histological analysis of the rat CN's and theoretical thermal damage model will be demonstrated as a more definitive indicator of thermal damage.

4.5 Conclusions

A novel all-single-mode-fiber design for optical stimulation of the rat cavernous nerves, using CW infrared laser radiation, was successfully tested. This approach has several advantages including: lower cost, elimination of alignment and maintenance issues, and an improved spatial beam profile. With further development, this design may be useful for safe and reproducible noncontact optical stimulation of the cavernous nerves during prostate cancer surgery.

CHAPTER 5: SUBSURFACE OPTICAL STIMULATION OF THE RAT PROSTATE NERVES USING CONTINUOUS-WAVE NEAR-INFRARED LASER RADIATION

5.1 Introduction and Background

As demonstrated in the previous Chapters 3 and 4, we have studied ONS as an alternative to electrical nerve stimulation of the CN's in the rat model, in vivo. The rat model is an ideal, inexpensive laboratory model because the CN's is of similar size to the human CN's, and it is directly visible and easily identifiable on the surface of the prostate [48].

However, successful translation of ONS into the clinic as an intra-operative diagnostic tool for identification and preservation of the human CN's during prostate cancer surgery will require demonstrating feasibility in a tissue model more closely resembling that of the human prostate anatomy. Most notably, the human cavernous nerve is not directly visible on the prostate surface, but rather lies below a thin layer of fascia. Figure 5.1 shows a representative photograph of the prostate gland surrounded by a fascia layer. It is the ability of ONS to detect and locate the CN below a thin fascia layer that would be most valuable in the clinic.

In this chapter, we report subsurface optical stimulation of the rat CN's study to determine whether ONS can be used for subsurface detection of the CN in a rat prostate model when a thin layer of fascia is placed over the CN and onto the surface of the prostate gland.

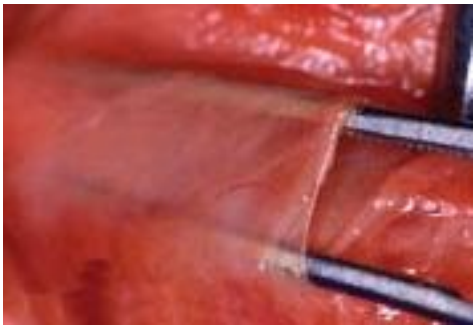

Figure 5.1: A photograph of the thin periprostatic levator fascia layer over the surface of the cavernous nerves and prostate gland, varying from 100 - 300 μm in thickness [49].

5.2 Experimental Setup

All animal experiments were performed in vivo using eight adult male Sprague Dawley rats (400 to 600 g) in the Neurourology laboratory at Johns Hopkins Hospital (Baltimore, MD). Animal preparation, surgical procedure, and animal protocol were similarly performed as explained previously in Chapter 3 (Figure 3.2).

Two pigtailed single-mode near-infrared diode lasers were used in this study: The first laser emitted up to 150 mW of power at a wavelength of 1455 nm. Laser radiation at 1455 nm has an OPD of around 350 μm in water (the dominant soft tissue absorber in the near-infrared), shown in Figure 3.1, which closely matches the rat CN diameter of 200 to 400 μm for uniform irradiation of the nerve as previously described in Chapter 3. The 1455 nm laser was used for two purposes: to demonstrate robust ONS prior to placement of the fascia layer over the CN and then to determine the limits of this wavelength in ONS as a function of fascia thickness.

A 500 mW diode laser (Brightlase-7115, Laser Operations LLC, Sylmar, CA) emitting at a wavelength of 1550 nm was used as a second laser in the subsurface stimulation study. Laser radiation at this wavelength has an OPD of ~ 930 μm in water

(Figure 3.1). The purpose of using this more deeply penetrating wavelength was to determine the limits of subsurface ONS of the rat CN's when a thicker layer of fascia was present. Figure 5.2 provides a photograph of the all-single-mode-fiber design, laparoscopic probe, and details of the optical components.

For both lasers, the experimental setup was similar to that described in Chapter 4 (Figure 4.2): a red diode laser (660 nm) aiming beam was coupled into a single mode fiber.

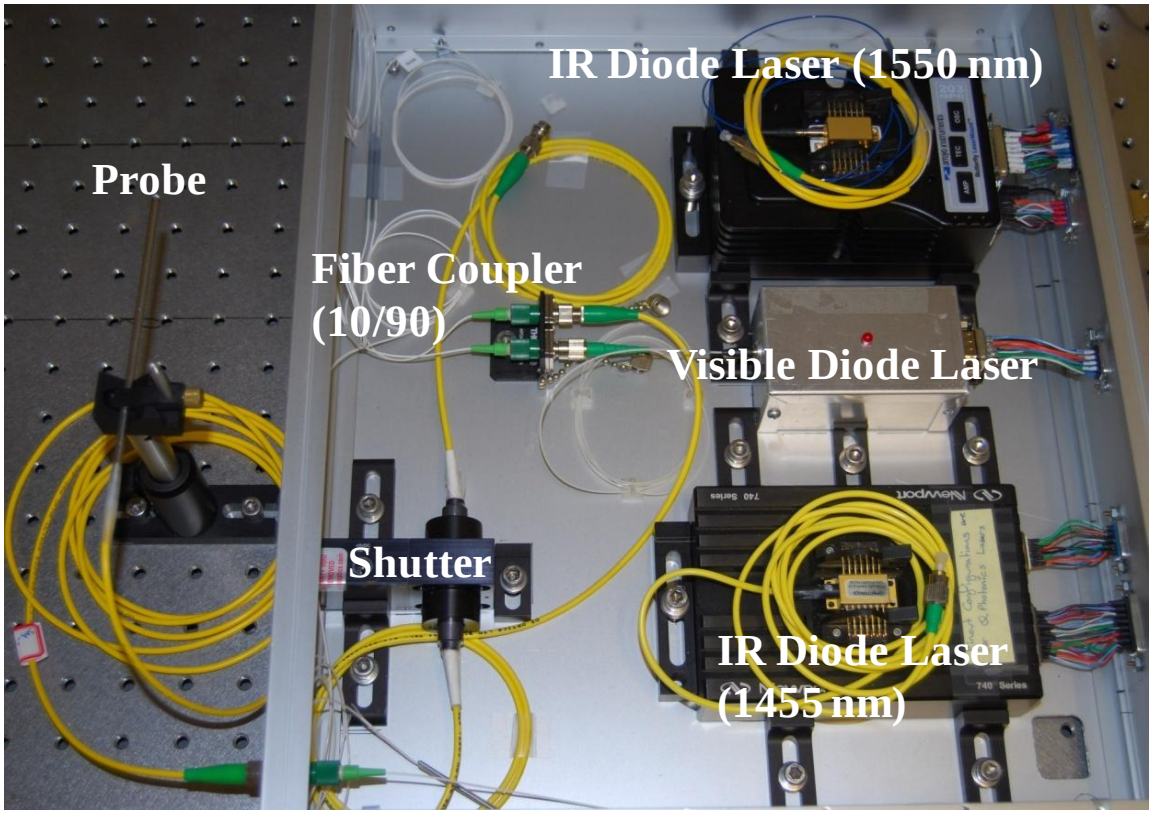

Figure 5.2: Custom-built, laparoscopic laser probe and compact optical nerve stimulation system using visible diode laser and near-infrared diode lasers, single-mode optical fiber, and other standard, inexpensive and mass-produced telecommunication components. The diode controllers for the visible and infrared lasers are not shown.

An SMF coupler with a 10/90 coupling ratio combined both visible and infrared laser beams into a single SMF. An in-line optical shutter in the infrared laser SMF arm provided rapid on/off switching of the laser beam during stimulation. The fiber coupler output was connected to a custom-built 10-Fr (3.4-mm-OD) laparoscopic probe consisting of standard single-mode fiber optic cable with an aspheric lens attached to the distal tip for beam collimation. Design and assembly details of the probe have been previously reported in Chapter 2. This probe provided a collimated 1-mm diameter Gaussian laser beam over a working distance of approximately 15 mm, as characterized in Figures 2.2b and 2.3b.

5.3 Experimental Procedure

The following sequence of steps was used in the optical stimulation experiments. First, the visible aiming beam was used to align the 1-mm-diameter infrared laser beam with the exposed rat CN. Second, ONS was performed to determine the threshold laser power for stimulation by slowly escalating the laser power and repeating stimulation. Third, a thin layer of fascia from the rat testicle was carefully dissected and placed directly over the CN on the surface of the prostate, as shown in Figure 5.3. Fourth, an optical coherence tomography (OCT) system (Niris, Imalux, Cleveland, OH) was used to noninvasively image and measure the thickness of the fascia layer with an accuracy of approximately 10 μm (Figure 5.5). Fifth, subsurface ONS was performed again by slowly escalating the laser power in small increments until the threshold for stimulation was reached, as confirmed by an ICP response in the rat penis.

5.4 Results

Successful optical stimulation of the rat CN with CW laser radiation at a wavelength of 1550 nm was achieved through a fascia layer with a thickness up to about 450 µm. However, there was a significant decrease in the magnitude and speed of ICP response between optical stimulation of the CN's on the surface versus subsurface stimulation with a layer of fascia present, overlying the CN's. The difference in response time between surface and subsurface ONS was measured to be approximately 2 - 3 s. The difference in magnitude and shape of the ICP responses both between surface and subsurface stimulation studies and within each study as well, fluctuates and is dependent on anatomical and physiological parameters (e.g. nerve dimensions and blood pressure). Figure 5.4 provides a representative range of ICP responses obtained in the rat penis with surface stimulation and repeated subsurface stimulations in a single rat. For the purposes of developing ONS as a potential intra-operative diagnostic method, an ICP response significantly above the baseline would be sufficient for positive identification of the CN during prostate surgery, as demonstrated in this current study.

As the thickness of the fascia was increased from 85 - 600 µm, the threshold laser power for reliable and reproducible optical stimulation also increased (Table 5.1). Successful ONS was observed at 1455 nm through a thin fascia layer measuring up to around 110 µm thick. However, when the fascia layer was increased to a thickness of 240 µm, no ICP response was measured with the diode laser emitting laser radiation at a wavelength of 1455 nm, and visible thermal damage to the fascia was observed at a power of 60 mW, corresponding to a peak temperature of ~ 48 ^{o}C on the fascia surface.

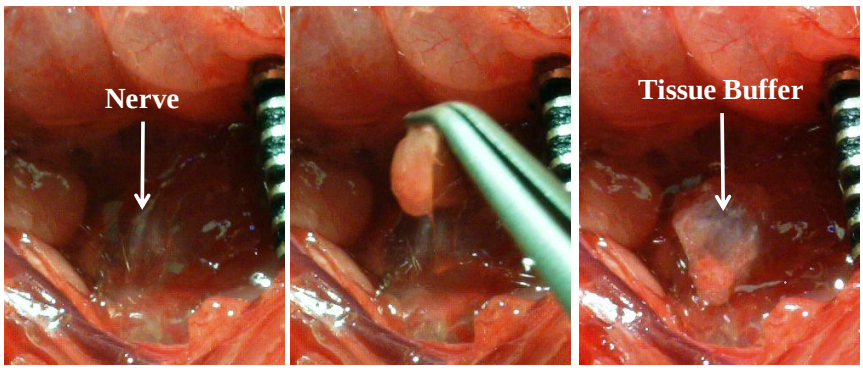

Figure 5.3: A thin layer of fascia from the testicle was dissected and placed on top of the cavernous nerve in a rat prostate model to simulate the fascia layer that would be present over the cavernous nerves in the human anatomy, for potential clinical application.

Table 5.1: Subsurface optical nerve stimulation threshold parameters for the rat CN as a function of laser wavelength and fascia layer thickness.

	Fascia Thickness (µm)					
Parameter (1455 nm/1550 nm)	**80-90**	**100-110**	**230-240**	**300-320**	**420-450**	**600-620**
Power to stimulate (mW):	33/NA	45/NA	No Stim./45	No Stim./60	No Stim./80	No Stim./No Stim.
Threshold ICP reponse time (s):	13.8±0.3/NA	14.4±0.5/NA	No Stim./14.8±0.3	No Stim./14.1±0.3	No Stim./13.1±0.5	No Stim./No Stim.
Total energy to stimulate (J):	0.46/NA	0.65/NA	No Stim./0.67	No Stim./0.85	No Stim./1.05	No Stim./No Stim.
Fluence to stimulate (J/cm^2):	58.6/NA	82.8/NA	No Stim./85.4	No Stim./108.3	No Stim./133.8	No Stim./No Stim.
Temperature on fascia (^{o}C):	41.1±0.5/NA	41.5±0.5/NA	No Stim./40.2±0.3	No Stim./44.8±0.9	No Stim./45.0±0.6	No Stim./No Stim.

*NA=Not applicable
*ICP=Intracavernous pressure

The OPD at 1455 nm is around 350 µm, so when the thickness of the CN (200 - 400 µm) is also added to the fascia thickness, the CN depth is beyond the OPD for 1455 nm. Therefore, the failure to stimulate the CN with the 1455 nm laser and a fascia layer of ~ 240 µm and greater was expected. Figure 5.5 provides images of fascia layers taken by the OCT system, the optical stimulation threshold power for different fascia thicknesses increasing from 85 µm to 600 µm, and representative ICP responses for each fascia thickness.

For thicker fascia layers (240 - 600 µm), the 1550 nm laser with an OPD of approximately 930 µm was substituted for the 1455 nm laser. Successful ONS was achieved in fascia layers up to 450 µm thick, but no ICP response was detected for a 600 µm fascia layer. A threshold laser power of 45 mW was necessary for 240 µm fascia layer versus 80 mW for the 450 µm fascia layer. Although the 1550 nm laser was capable of output powers up to 500 mW, thermal damage to the fascia layer was observed when the laser power was increased to 90 mW for the 600 µm fascia layer, corresponding to a peak temperature of ~ 53 ^{o}C on the fascia surface. The thickest fascia layer in which successful ONS was observed at 1550 nm was about 450 µm which corresponded to a laser power of 80 mW at the threshold for stimulation and a temperature of ~ 45 ^{o}C at the surface of the fascia.

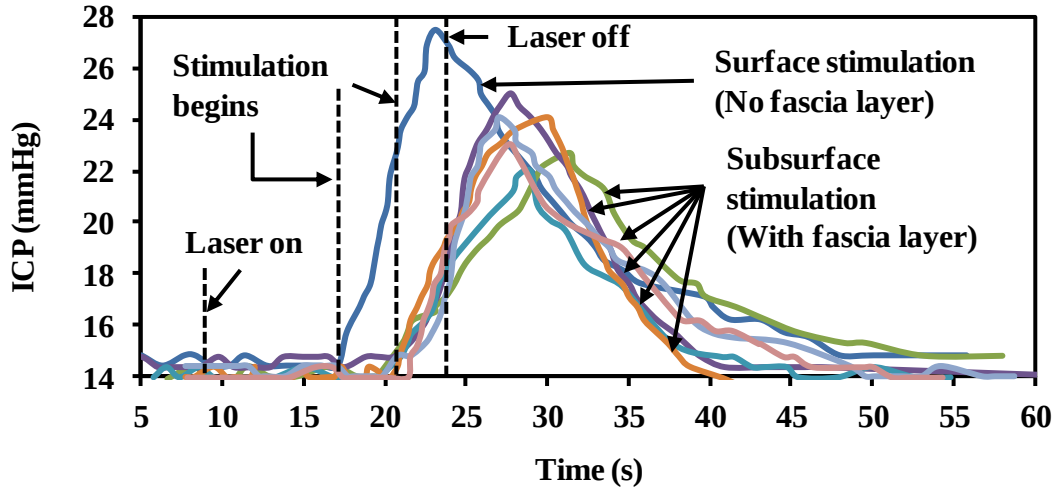

Figure 5.4: Surface ONS was first performed, as a control, before then placing the fascia layer over the cavernous nerve for subsurface stimulation. Although subsurface optical stimulation of the rat cavernous nerves was reproducible, as shown by the six individual stimulations performed, the intracavernous pressure (ICP) response was significantly weaker and slower than ONS without the fascia layer. Tissue thickness = 450 µm. Laser Parameters; wavelength = 1550 nm, power = 80 mW.

5.5 Discussion and Conclusions

Limited knowledge of the location and path of the CN's on the prostate surface, which are responsible for sexual function, has made preservation of the CN's during prostate cancer surgery challenging. Implementation of new technologies which are capable of improved identification and detection of the CN's during surgery would aid in preservation of the CN's and result in improved post-operative sexual function and patient quality-of-life.

The preliminary subsurface stimulation study reported in this chapter demonstrates the feasibility of optical stimulation and identification of the rat prostate cavernous nerve when it lies beneath a thin layer of fascia, approximating the human anatomy during prostate cancer surgery. While a near-infrared laser operating at a wavelength of 1455 nm has proven successful in previous studies (Chapter 3) for ONS of the exposed rat CN [28], the optical penetration depth (~ 350 μm) at this wavelength was not sufficient to successfully stimulate the nerve when it was beneath a fascia layer thickness of ~ 240 μm or greater. Therefore, it was necessary to switch to the 1550 nm laser wavelength, which has an OPD of ~ 930 μm in water, for successfully, reliable and reproducible optical stimulation of the CN in fascia layers at up to around 450 μm thick.

While the thickness of the fascia layer overlying the CN's in the human prostate is variable, previous detailed anatomic studies of the CN's in fresh human cadavers have revealed that the fascia layer varies from 100 - 300 μm in thickness [32]. It should be noted that typically there is some shrinkage of tissue during histologic processing, and that these values may slightly underestimate the true thickness of the fascia layer. However, other studies using OCT to image the human CN and prostate, in vivo, have

shown comparable dimensions for the fascia layer [33-34]. Therefore, demonstration of ONS of the rat CN through a fascia layer up to at least 450 µm in this study shows promise for future clinical translation of this ONS method into the human as well.

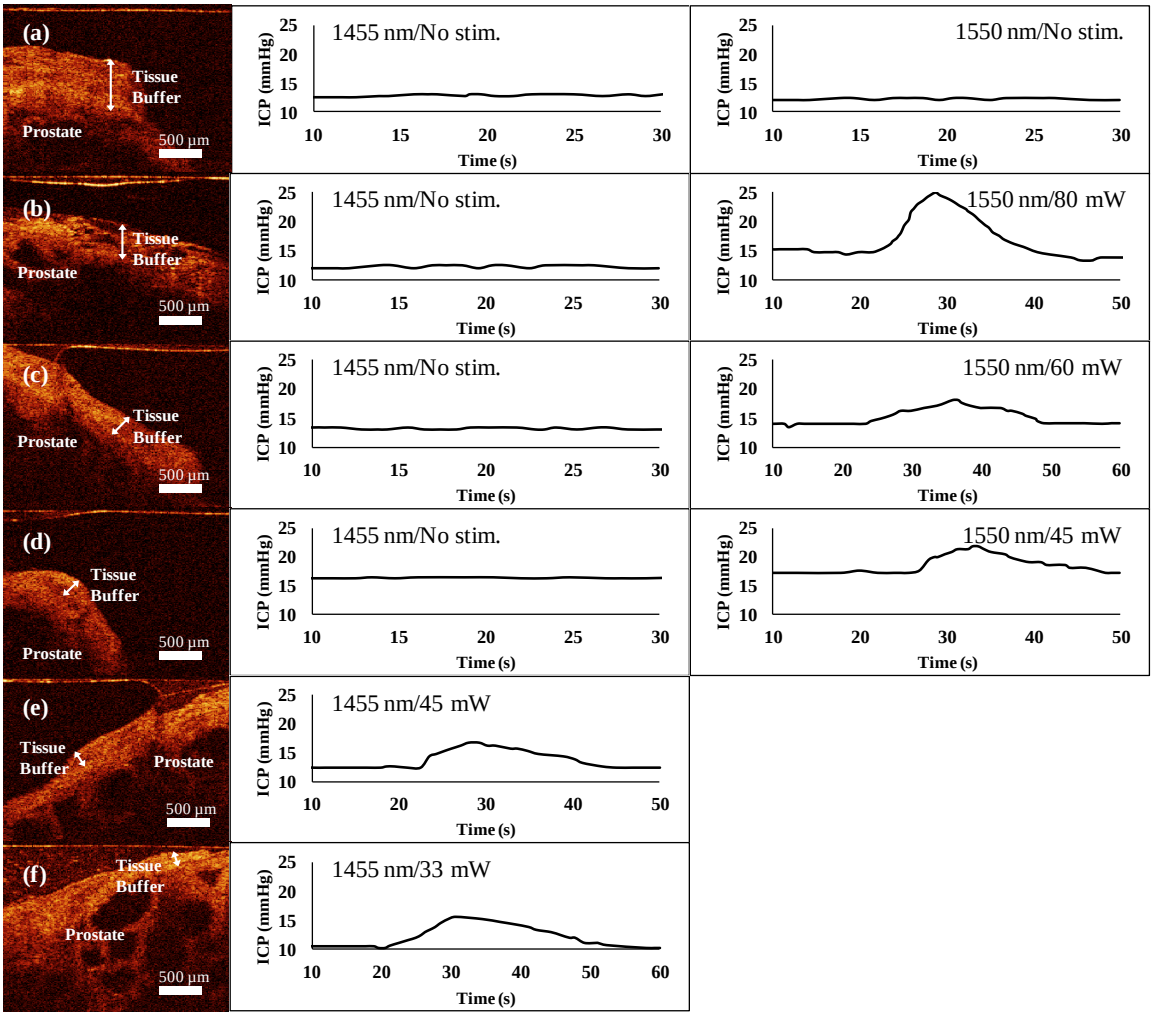

Figure 5.5: Optical nerve stimulation threshold power (mW) for stimulation of the rat cavernous nerves as a function of laser wavelength (nm) and fascia layer thickness (µm). Optical coherence tomography (OCT) was used to noninvasively measure the thickness of the fascia layer placed over the cavernous nerve and prostate. The white arrows mark the tissue thickness at the exact location where the laser beam was aligned for optical nerve stimulation in the images taken with the OCT system: (a) 600 µm, (b) 450 µm, (c) 300 µm, (d) 240 µm, (e) 110 µm, and (f) 85 µm.

There were several limitations encountered during subsurface ONS studies. First, use of a laser wavelength with a higher OPD was necessary for sufficient optical energy to pass through the fascia layer to the CN and provide the threshold temperature for initiating nerve activation. However, light scattering becomes a more important factor in the attenuation of the beam with depth. Thus, optical diffusion of the photons, by definition, may result in this technique being slightly less selective in identifying the exact location of the nerve. Second, since the laser beam is attenuated with depth, a higher laser power was necessary in order to deposit sufficient energy at the depth of the CN for successful stimulation. At some point, the temperature gradient with tissue depth limited the ability to stimulate nerves without thermally damaging the overlying fascia layer. This limitation appeared to be encountered during studies in which a 600-µm-thick fascia layer was placed over the nerve. Finally, as the fascia layer thickness was increased from 85 - 600 µm, both slower and weaker ICP response was observed. Thus, challenges still remain with further optimization of the laser parameters necessary to provide a rapid and robust ICP response that is sufficient in a clinical setting for ONS to be used as a reliable and reproducible intra-operative method for identification and preservation of the CN. Nevertheless, this preliminary study demonstrates the feasibility of subsurface ONS.

It should be noted that although the wavelengths of 1450 and 1550 nm have been used previously for ONS, those lasers were relatively expensive, high power, pulsed laser systems [47]. In this study, on the contrary, relatively inexpensive, low power, CW, single-mode diode lasers were integrated into a compact, all-single-mode ONS system for the experiments.

In summary, this preliminary study has demonstrated, for the first time, subsurface optical stimulation of the rat prostate cavernous nerve using infrared laser energy in a pre-clinical model closely simulating the human anatomy. With further development, optical nerve stimulation may be a useful technique for intra-operative identification and preservation of the cavernous nerves during prostate cancer surgery.

CHAPTER 6: COMPARISON OF EXPERIMENTAL DATA AND THERMAL DAMAGE MODEL FOR CAVERNOUS NERVES

6.1 Introduction

Determination of the threshold temperature for thermal damage to the nerve is as critical and essential as accurately defining the minimum amount of total laser energy, or stimulation threshold, required to provide reliable, reproducible and nerve stimulation with CW infrared laser radiation.

Previous studies have reported that the therapeutic window for nerve stimulation using pulsed infrared laser radiation had a relatively narrow range of ~ 0.35 to 0.9 J/cm^2 [19, 31] for safe and consistent stimulation without thermal damage to the nerve. This narrow therapeutic range is a major limitation of nerve stimulation with the use of infrared laser radiation. However, after optimization of the laser stimulation parameters and improvements in the fiber optic probe and laser spatial beam profile, stimulation of the rat CN at lower energies has been achieved successfully as explained in detail in Chapters 3 and 4.

In order to define the upper limit of this wider therapeutic window for optical stimulation of CN in a rat model, in vivo, identification of the thermal damage threshold for the nerve after laser irradiation will be investigated in this chapter by making a direct comparison of the visible thermal damage data, shown in Figure 4.4, with a theoretical thermal damage model.

6.2 Thermal Damage Model

A mathematical description of the cellular damage process in neural tissue is useful for predicting and characterizing thermal injury in response to laser irradiation during ONS. In addition, it will provide feedback for comparison with experimental results, based on nerve function (e.g. decay in ICP response time and magnitude) on repeated stimulation and visible observation of thermal damage to the CN surface, in order to optimize and accurately define the upper threshold for avoiding irreversible thermal damage to the nerve.

Thermal damage, typically quantified by a single parameter, $\Omega(t)$, can be evaluated using a model based on an Arrhenius integral [50]:

$$\Omega(t) = \zeta \int_0^{\tau} \exp\left(-\frac{E_a}{RT(t)}\right) dt \tag{6.1}$$

where ζ (s^{-1}) is a frequency factor; τ (s) is the total heating time; E_a (J/mol) is an activation energy of the transformation; R (8.32 J/K mol) is the universal gas constant; and $T(t)$ is the absolute temperature of the tissue in degrees Kelvin. Numerical values of frequency factor (ζ) and activation energy (E_a), corresponding to the amount of energy needed to start the transformation process, can be derived from experimental analysis.

As shown in Eq. 6.1, the thermal damage parameter $\Omega(t)$ depends exponentially on temperature and linearly on heating time, and can also be expressed as a damage probability given by:

$$Damage(\%) = 100 \times (1 - \exp(-\Omega(t)) . \tag{6.2}$$

By using Eq. 6.2, the damage probability is calculated to be 0% for a damage parameter of 0, 63% for a damage parameter of 1, and 99% for a damage parameter of 4.6.

The damage parameter shows a linear increase with increasing exposure time for a constant temperature during irradiation. This linear relationship is used to calculate the frequency factor and the activation energy by means of fitting experimental results to the Arrhenius integral (Eq. 6.1). When $\Omega(\tau)$ is equal to 1 (the damage probability of 63%), Eq. 6.1 can be written in a new format for a constant temperature exposure as follows:

$$\ln(\tau) = (\frac{E_a}{R})\frac{1}{T} - \ln(\zeta)\,. \tag{6.3}$$

Plotting an $\ln(\tau)$ versus $1/T$ graph with the experimental data will yield a slope equal to E_a/R and y-intercept corresponding to $-\ln(\zeta)$ from which the frequency factor and the activation energy can both be determined, respectively.

For purposes of discussion and possible comparison with experimental temperature feedback taken by a thermal camera during ONS, it is useful to define the critical temperature at which damage accumulation rate, $\Delta\Omega/\Delta t$:

$$\frac{\Delta\Omega}{\Delta t} = \zeta \exp(-\frac{E_a}{RT_{crit}})\,. \tag{6.4}$$

The importance of the critical temperature is related to the thermal damage parameter, frequency factor, and activation energy. Below this critical temperature, or thermal damage threshold temperature, the rate of damage accumulation is negligible. However, the damage rate increases exponentially when this value is exceeded.

Table 6.1summarizes all estimated values of the rate process coefficients of thermal tissue damage, frequency factor and activation energy, for specific tissue types. We examined these coefficients, previously estimated by other researchers, to predict tissue damage and cell death. Afterwards we selected the parameter set in terms of determining critical temperature to compare with our experimental and calculated results.

6.3 Results and Discussion

The precise mechanism of ONS is still not well understood. However, since the laser is operated at an infrared wavelength in CW mode for our nerve stimulation studies (Chapters 3 and 4); we can conclude that the mechanism for ONS from laser-tissue interaction is believed to be photothermal. Thus, tissue damage mainly occurs in the form of thermal damage to the nerve after the short-term optical stimulation is completed.

The minimum incident laser power and irradiance required for reproducible and reliable laser stimulation of the rat CN with CW infrared laser radiation were successfully determined (Chapter 4). The average stimulation threshold irradiance was calculated to be 3.6 ± 0.7 W/cm^2 and 3.9 ± 0.3 W/cm^2 with the use of a Gaussian spatial beam profile and the flat-top spatial beam profile, respectively. As a complementary study, we also focused on determining the maximum value of the various laser parameters including: surface temperature, average incident power and irradiance that could be used to define the therapeutic window of our ONS technique.

Several thermal tissue damage models and Arrhenius rate process coefficients from the literature have been reported by other researchers. However, to the best of our knowledge, there is no data either on the coefficients, frequency factor and activation energy, or thermal damage model for nerve tissue. The damage threshold temperature, previously observed at the end of optical stimulation of the rat CN's, is close to the critical temperature predicted with rate process coefficients reported by Sramek et al. [51] (Table 6.1).

Table 6.1: Published rate process coefficients (activation energy, E_a, and frequency factor, ζ) of thermal tissue damage for specific tissues.

E_a (J mol^{-1})	ζ (s^{-1})	Tissue Types
1.74 x 10^6	7.00 x 10^{282}	Fibroblast Cell [52]
5.06 x 10^5	2.98 x 10^{80}	Baby Hamster Kidney Cell [53]
6.28 x 10^5	3.10 x 10^{99}	Retina [54]
2.40 x 10^5	2.90 x 10^{37}	Skeletal Muscle Cell [55]
3.40 x 10^5	1.60 x 10^{55}	Retina Cell [51]
9.70 x 10^4	1.50 x 10^{16}	Mouse Embryonic Fibroblast Cell [56]
6.28 x 10^5	3.10 x 10^{98}	Tumor Cell [57]
2.87 x 10^5	4.36 x 10^{43}	Human Renal Carcinoma [58]
6.30 x 10^5	3.10 x 10^{98}	Porcine Skin [50]
6.27 x 10^5	3.10 x 10^{98}	Human Skin [59]
4.18 x 10^5	4.32 x 10^{64}	Pig Skin [60]

In this chapter, we specifically seek to verify an expression for the critical threshold temperature to provide safe and effective optical stimulation of nerve tissue. In our analysis here, the generalized Arrhenius integral (Eq. 6.1) which consists of three rate process coefficients (frequency factor, ζ, activation energy, E_a, and universal gas constant, R) is used to estimate the critical temperature that causes irreversible thermal damage. To illustrate how our damage threshold temperature observed during 15 s laser irradiation is comparable to the estimated value, we also examine the thermal damage parameter, $\Omega(t)$, as a function of time.

In Figure 6.1, the temperature data resulting in visible thermal damage to the nerve mentioned in Chapter 4 is plotted on an $\ln(\tau)$ versus $1/T$ graph as shown in Eq. 6.3. As previously reported in Table 4.1, the average incident laser power to damage the rat CN is approximately 55 mW corresponding to an irradiance of 7 W/cm^2 for a beam diameter of 1 mm. The critical temperature threshold to damage the CN is measured to be ~ 48.5 ^{o}C and the exposure time is 15 s.

A linear-fit line (solid line) is fitted through the experimental temperature data in the graph. Then, the slope of the line and y-intercept are derived to estimate the value of the coefficients; frequency factor (ζ) is 8.22 x 10^{36} s^{-1} and activation energy (E_a) is 2.24 x 10^5 J mol^{-1}. Figure 6.1 also compares our experimental results to the linear-fit line (dashed line) drawn with numerical values for the frequency factor and the activation energy given as: ζ = 1.6 x 10^{55} s^{-1}; E_a = 3.4 x 10^5 J mol^{-1} [51].

Typical temperature measurement obtained from nerve surface during 15 s laser radiation with the laser power of ~ 55 mW and the damage parameter $\Omega(t)$ calculated at the surface of the heated nerve by using Eq. 6.4 are shown in Figure 6.2. The initial surface temperature of the rat CN is around 34 ^{o}C. As expected, the surface temperature increases as a function of time, reaches a maximum value of ~ 48.3 ^{o}C, and then decays after the laser is turned off due to heat diffusion into the surrounding tissue and air.

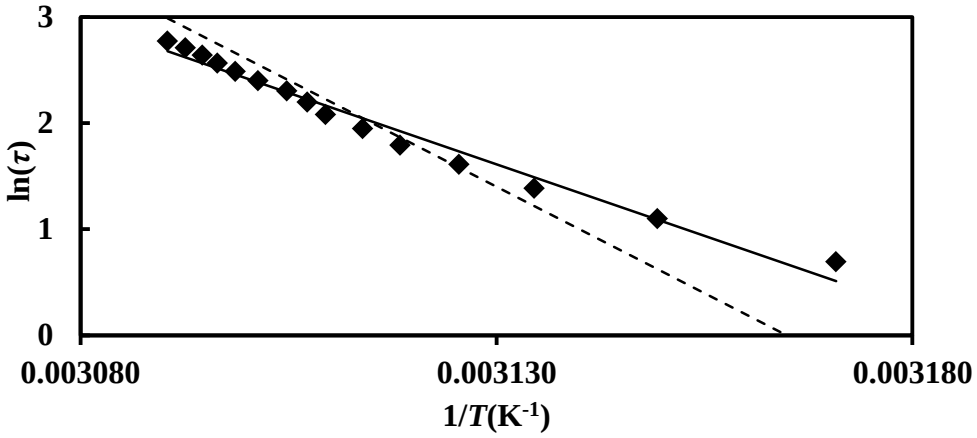

Figure 6.1: Plot of the natural logarithm of the exposure time (τ) at which $\Omega(\tau)$ = 1 versus $1/T$ (K^{-1}) . Frequency factor (ζ) and activation energy (E_a) are calculated from the slope and the y-intercept of a linear-fit line (solid line), respectively. ζ = 8.22 x 10^{36} s^{-1} and E_a = 2.24 x 10^5 J mol^{-1}. Dashed line shows the linear-best-fit calculated with Arrhenius rate process coefficients (Table 6.1), previously published by Sramek et al., for comparison with our experimental data.

As seen in Figure 6.2, the damage parameter $\Omega(t)$ remains low until the surface temperature rises to ~ 47.5 ^{o}C. When the temperature exceeds ~ 48 ^{o}C, the value of the damage parameter $\Omega(t)$ increases very rapidly and continues to rise even after the laser is turned off. The maximum damage parameter is calculated to be about 3.2 at the end of stimulation, significantly above the critical damage parameter of 1 which results in irreversible damage to the biological tissue. By using Eq. 6.2, the damage probability is calculated to be 97% for experimental data with the rate process coefficients determined from Figure 6.1.

For comparison, the damage parameter calculated with the rate coefficients determined experimentally by Sramek et al. for retinal pigment epithelial cell is also considered in Figure 6.2. It reaches the maximum value of approximately 2.9, corresponding to the damage probability of 93%.

From these graphs, a linear-fit line yielded a frequency factor and activation energy for the rate process coefficients that describes the Arrhenius behavior of the system, and thermal damage in laser irradiated nerve tissue was investigated as a function of time. The resulting frequency factor and activation energy are $\zeta = 8.22 \times 10^{36}$ s^{-1} and $E_a = 2.24 \times 10^{5}$ J mol^{-1}, respectively. By substituting these calculated coefficients into Eq. 6.4, the critical temperature to damage the rat CN is estimated to be ~ 47.5 ^{o}C. As a further verification of the model by a quantitative comparison, the calculated result is in general agreement with the damage threshold temperature of around 48.5 ^{o}C, obtained from optical stimulation of the rat CN experiments.

When comparing our theoretical data with published values of two Arrhenius coefficients ($\zeta = 1.6 \times 10^{55}$ s^{-1} and $E_a = 3.4 \times 10^{5}$ J mol^{-1}) [51] for retina cell death model,

it is clear that although the activation energy (E_a) values are on the same order of magnitude, the frequency factor values (ζ) are slightly different. However, very good agreement is obtained between the model prediction (~ 47.5 ^{o}C) and critical temperature of ~ 47.3 ^{o}C calculated with the use of these two rate coefficients proposed by Sramek et al. into Eq. 6.4.

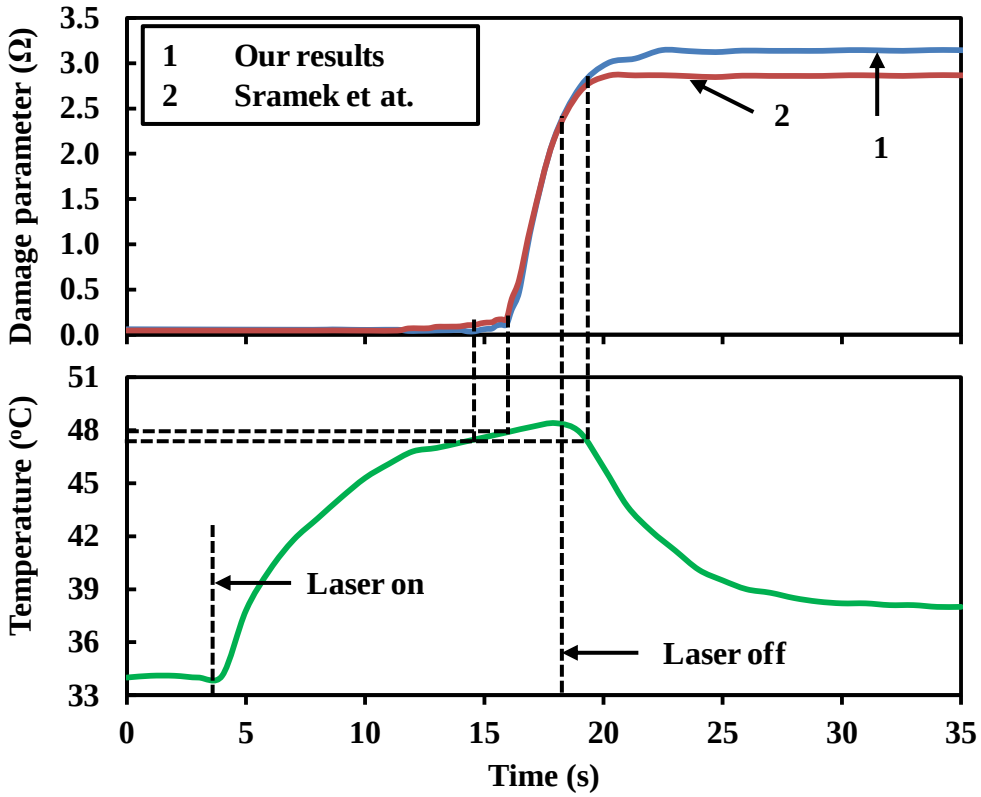

Figure 6.2: Temperature and damage parameter (Ω) of the laser irradiated rat CN's during 15 s of optical stimulation with CW infrared laser beam as a function of time. The surface of the CN reaches a temperature of ~ 48 ^{o}C after 12 s of laser radiation, closely corresponding to the onset of the sharp increase in Ω. In comparison, the damage parameter reported for retina cell death model by Sramek et al. and estimated Arrhenius coefficients is calculated to be 3.2 and 2.9 at the end of the short-term (15 s) optical stimulation of the rat CN, respectively. Both values are significantly higher than the critical damage parameter (Ω = 1) which indicates irreversible thermal damage of biological tissue.

Although the estimated Arrhenius rate process coefficient values and critical temperature threshold in the model are comparable, there are important limitations to precisely predict the thermal damage threshold to the rat CN.

First, the Arrhenius integral is predominantly used to characterize thermal damage to biological tissue with the use of direct measurements of protein denaturation by means of scattering increase. In contrast, it should be noted that this rate formulation does not take into account the nonlinear response of the tissue to photothermal effects.

Second, optical properties of nerve tissue change dynamically during laser irradiation. Thus, it is important to study the effects of these different optical properties on thermal damage and critical temperature estimations using well-known Monte Carlo methods. In addition, it may be necessary to investigate the complex tissue geometry in (2D and 3D) to analyze rigorously analyze the heat distribution resulting from the laser-tissue interaction.

Third, it is only possible to measure the surface temperature of the nerve by using a thermal camera as described in the previous chapters. However, the specifically the highest tissue temperature does not occur right at the tissue surface, but rather just below the tissue surface for two reasons. Back-scattering of the light contributes to a higher fluence just below the surface and convective air cooling of the tissue surface keeps it slightly cooler than below the surface.

Finally, more rigorous histological analysis of thermal damage to the nerve combined with a theoretical thermal damage model is needed to determine the optimal therapeutic window for safe, consistent and reliable ONS.

6.4 Conclusions

In this chapter, we evaluated the damage threshold for optical stimulation of the rat CN's with CW infrared laser radiation by correlating gross experimental observations with direct comparison to a theoretical thermal damage model using the Arrhenius integral and previously reported results in the literature. A calculation consisting of Arrhenius rate process coefficients, frequency factor (ζ) and activation energy (E_a), damage parameter ($\Omega(t)$), and critical temperature (T_{crit}) to damage to the nerve tissue was performed. For comparison of the values of the damage threshold temperature, we obtained general agreement between published results, experimental results and, calculated values using the Arrhenius integral for the data of our actual experiment.

CHAPTER 7: CONCLUSIONS

This chapter summarized the contributions of this thesis in the field of Optical Nerve Stimulation of the rat cavernous nerves on the prostate gland surface.

7.1 Summary

Optical Nerve Stimulation (ONS) of the rat cavernous nerves (CN's) on the prostate gland surface has been studied in five steps: (1) developed a compact optical laparoscopic probe for ONS studies in vivo rat model; (2) demonstrated, for the first time, surface optical stimulation of the CN's in the rat with the use of continuous-wave infrared laser radiation; (3) developed a compact, inexpensive all-single-mode-fiber design; (4) shown, for the first time, subsurface ONS of the rat prostate nerves; (5) investigated the upper temperature limit at where the CN is damaged during ONS.

First, three different laparoscopic laser probes were designed and assembled for use in optical stimulation of the CN's in a rat model. All of these probes fit through standard, 5-mm-ID, laparoscopic port, are capable of scanning a collimated 1-mm-diameter laser spot across the prostate surface. A laser probe consisting of a multimode optical fiber (200-μm-core-diameter) was used for ONS with a Gaussian infrared laser radiation at the wavelength of 1870 nm. The other two improved ONS probes, providing collimated Gaussian and flat-top laser radiations were built with the use of a 9-μm-core single-mode fiber, respectively, and used with 1455-nm and 1550-nm diode lasers.

Second, a direct comparison in terms of response time of intracavernous pressure (ICP) response was made between a Thulium fiber laser (1870 nm) operated in pulse mode and in continuous-wave mode. The fastest ICP response was produced by using continuous-wave infrared laser radiation, providing the fastest increase in temperature from baseline to above the CN's stimulation threshold temperature of ~ 42 ^{o}C, as compared to pulsed irradiation with pulse duration of 5 ms.

Third, a compact, inexpensive all-single-mode-fiber configuration was designed and successfully tested in optical stimulation of the rat CN's studies. This design consists of two different pigtailed single-mode laser diodes at the wavelength of 1455 nm for surface ONS and 1550 nm for subsurface ONS, respectively. In addition, this approach introduces an advantage in elimination of alignment and maintenance issues.

Fourth, successful optical stimulation of CN's in a rat model was achieved through a fascia thickness up to around 450 μm. The 1550-nm laser with an optical penetration depth of ~ 930 μm in water was utilized for the thicker fascia layers of ~ 240 - 600 μm. The thickness of periprostatic levator fascia layer overlying CN's in the human prostate varies from 100 - 300 μm in thickness. Therefore, demonstration of ONS of the rat CN's through a fascia layer in this study shows promise for future clinical translation of this ONS method into the human as well.

Fifth, general agreement between published result, experimental result and, estimated result using the Arrhenius integral for the data of our actual experiment was successfully obtained in order for comparison of the values of the damage threshold temperature.

BIBLIOGRAPHY

[1] P. C. Walsh, "Anatomical studies of the neurovascular bundle and cavernosal nerves," *J Urol,* vol. 174, p. 566, Aug 2005.

[2] A. L. Burnett, G. Aus, E. D. Canby-Hagino, M. S. Cookson, A. V. D'Amico, R. R. Dmochowski, D. T. Eton, J. D. Forman, S. L. Goldenberg, J. Hernandez, C. S. Higano, S. Kraus, M. Liebert, J. W. Moul, C. Tangen, J. B. Thrasher, and I. Thompson, "Erectile function outcome reporting after clinically localized prostate cancer treatment," *J Urol,* vol. 178, pp. 597-601, Aug 2007.

[3] O. Kaufmann, J. Claro, J. Cury, E. Andrade, B. Longo, W. Aguiar, L. Mello, and M. Srougi, "The development of a rat model of erectile dysfunction after radical prostatectomy: preliminary findings," *Bju International,* vol. 102, pp. 1026-1028, Oct 2008.

[4] F. Rabbani, M. Patel, P. Cozzi, J. P. Mulhall, and P. T. Scardino, "Recovery of erectile function after radical prostatectomy is quantitatively related to the response to intraoperative cavernous nerve stimulation," *Bju International,* vol. 104, pp. 1252-1257, Nov 2009.

[5] L. A. Geddes, "Optimal Stimulus-Duration for Extracranial Cortical Stimulation," *Neurosurgery,* vol. 20, pp. 94-99, Jan 1987.

[6] L. Klotz, "Neurostimulation during radical prostatectomy: improving nerve-sparing techniques," *Semin Urol Oncol,* vol. 18, pp. 46-50, Feb 2000.

[7] H. L. Kim, D. S. Stoffel, D. A. Mhoon, and C. B. Brendler, "A positive CaverMap response poorly predicts recovery of potency after radical prostatectomy," *Urology,* vol. 56, pp. 561-564, Oct 2000.

[8] P. C. Walsh, P. Marschke, W. J. Catalona, H. Lepor, S. Martin, R. P. Myers, and M. S. Steiner, "Efficacy of first-generation Cavermap to verify location and function of cavernous nerves during radical prostatectomy: A multi-institutional evaluation by experienced surgeons," *Urology,* vol. 57, pp. 491-494, Mar 2001.

[9] J. Holzbeierlein, M. Peterson, and J. J. Smith, "Variability of results of cavernous nerve stimulation during radical prostatectomy," *J Urol,* vol. 165, pp. 108-10, Jan 2001.

[10] J. Wells, C. Kao, K. Mariappan, J. Albea, E. D. Jansen, P. Konrad, and A. Mahadevan-Jansen, "Optical stimulation of neural tissue in vivo," *Optics Letters,* vol. 30, pp. 504-506, Mar 1 2005.

[11] J. Wells, C. Kao, E. D. Jansen, P. Konrad, and A. Mahadevan-Jansen, "Application of infrared light for in vivo neural stimulation," *Journal of Biomedical Optics,* vol. 10, pp. -, Nov-Dec 2005.

[12] A. D. Izzo, C. P. Richter, E. D. Jansen, and J. T. Walsh, "Laser stimulation of the auditory nerve," *Lasers in Surgery and Medicine,* vol. 38, pp. 745-753, Sep 2006.

[13] J. Wells, P. Konrad, C. Kao, E. D. Jansen, and A. Mahadevan-Jansen, "Pulsed laser versus electrical energy for peripheral nerve stimulation," *Journal of Neuroscience Methods,* vol. 163, pp. 326-337, Jul 30 2007.

[14] A. D. Izzo, E. Suh, J. Pathria, J. T. Walsh, D. S. Whitlon, and C. P. Richter, "Selectivity of neural stimulation in the auditory system: a comparison of optic and electric stimuli," *Journal of Biomedical Optics,* vol. 12, pp. -, Mar-Apr 2007.

[15] C. P. Richter, R. Bayon, A. D. Izzo, M. Otting, E. Suh, S. Goyal, J. Hotaling, and J. T. Walsh, "Optical stimulation of auditory neurons: Effects of acute and chronic deafening," *Hearing Research,* vol. 242, pp. 42-51, Aug 2008.

[16] A. R. Duke, J. M. Cayce, J. D. Malphrus, P. Konrad, A. Mahadevan-Jansen, and E. D. Jansen, "Combined optical and electrical stimulation of neural tissue in vivo," *Journal of Biomedical Optics,* vol. 14, p. 060501, Nov-Dec 2009.

[17] S. Tozburun, G. A. Lagoda, A. L. Burnett, and N. M. Fried, "Continuous-wave Optical Stimulation of the Rat Prostate Nerves using an All-single-mode 1455 nm Diode Laser and Fiber System," *Proceedings of SPIE,* vol. 7883, pp. 1-6, 2011.

[18] S. Tozburun, G. A. Lagoda, M. Mayeh, A. L. Burnett, F. Farahi, and N. M. Fried, "Incorporation of Fiber Optic Beam Shaping into a Laparoscopic Probe for Laser Stimulation of the Cavernous Nerves," *Proceedings of SPIE,* vol. 754818, pp. 1-5, 2010.

[19] N. M. Fried, S. Rais-Bahrami, G. A. Lagoda, A. Y. Chuang, L. M. Su, and A. L. Burnett, "Identification and imaging of the nerves responsible for erectile function in rat prostate, in vivo, using optical nerve stimulation and optical coherence tomography," *IEEE Journal of Selected Topics in Quantum Electronics,* vol. 13, pp. 1641-1645, Nov-Dec 2007.

[20] N. M. Fried, G. A. Lagoda, N. J. Scott, L. M. Su, and A. L. Burnett, "Noncontact stimulation of the cavernous nerves in the rat prostate using a tunable-wavelength thulium fiber laser," *Journal of Endourology,* vol. 22, pp. 409-413, Mar 2008.

[21] S. Tozburun and N. M. Fried, "Design of a Compact Laparoscopic Probe for Optical Stimulation of the Cavernous Nerves," *Proceedings of SPIE,* vol. 716113, 2009.

[22] S. Tozburun, G. A. Lagoda, A. Burnett, and N. M. Fried, "Gaussian versus Flat-top Spatial Beam Profiles for Optical Stimulation of the Prostate Nerves," *Proceedings of SPIE,* vol. 7584W, pp. 1-6, 2010.

[23] S. Tozburun, M. Mayeh, G. A. Lagoda, F. Farahi, A. L. Burnett, and N. M. Fried, "A Compact Laparoscopic Probe for Optical Stimulation of the Prostate Nerves,"

IEEE Journal of Selected Topics in Quantum Electronics, vol. 16, pp. 941-945, Jul-Aug 2010.

[24] S. Tozburun, C. M. Cilip, G. A. Lagoda, A. L. Burnett, and N. M. Fried, "Continuous-wave infrared optical nerve stimulation for potential diagnostic applications," *Journal of Biomedical Optics,* vol. 15, Sep-Oct 2010.

[25] S. Tozburun, G. A. Lagoda, M. Mayeh, A. L. Burnett, F. Farahi, and N. M. Fried, "Incorporation of Fiber Optic Beam Shaping into a Laparoscopic Probe for Laser Stimulation of the Cavernous Nerves," *Proceedings of SPIE,* vol. 7548, pp. 1-5, 2010.

[26] S. Tozburun, C. M. Cilip, G. A. Lagoda, L. B. Arthur, and N. M. Fried, "Continuous-wave Pulsed Infrared Laser Stimulation of the Rat Prostate Cavernous Nerves," *Proceedings of SPIE,* vol. 7883, pp. 1-6, 2011.

[27] S. Tozburun, G. A. Lagoda, A. L. Burnett, F. Farahi, and N. M. Fried, "Fiber Beam Shaping for Optical Nerve Stimulation," *Proceedings of IEEE,* vol. 978-1-4244-8939-8, pp. 493-494, 2011.

[28] S. Tozburun, G. A. Lagoda, A. L. Burnett, and N. M. Fried, "Continuous-Wave Laser Stimulation of the Rat Prostate Cavernous Nerves Using a Compact and Inexpensive All Single Mode Optical Fiber System," *Journal of Endourology,* vol. 25, pp. 1727-1731, Nov 2011.

[29] S. Tozburun, G. A. Lagoda, A. L. Burnett, and N. M. Fried, "Subsurface Optical Stimulation of the Rat Prostate Nerves Using Continuous-wave Near-Infrared Laser Radiation," *Proceedings of SPIE,* vol. 8207, pp. 1-6, 2012.

[30] S. Tozburun, G. A. Lagoda, A. L. Burnett, and N. M. Fried, "Subsurface Near-infrared Laser Stimulation of the Periprostatic Cavernous Nerves," *Journal of Biophotonics,* vol. 10.1002, pp. 1-8, 2012.

[31] J. D. Wells, S. Thomsen, P. Whitaker, E. D. Jansen, C. C. Kao, P. E. Konrad, and A. Mahadevan-Jansen, "Optically mediated nerve stimulation: Identification of injury thresholds," *Lasers in Surgery and Medicine,* vol. 39, pp. 513-526, Jul 2007.

[32] A. Takenaka, G. Murakami, A. Matsubara, S. H. Han, and M. Fujisawa, "Variation in course of cavernous nerve with special reference to details of topographic relationships near prostatic apex: Histologic study using male cadavers," *Urology,* vol. 65, pp. 136-142, Jan 2005.

[33] M. Aron, J. H. Kaouk, N. J. Hegarty, J. R. Colombo, G. P. Haber, B. I. Chung, M. Zhou, and I. S. Gill, "Second prize: 2006 endourological society essay competition - Preliminary experience with the Niris (TM) optical coherence tomography system during laparoscopic and robotic prostatectomy," *Journal of Endourology,* vol. 21, pp. 814-818, Aug 2007.

[34] S. Rais-Bahrami, A. W. Levinson, N. M. Fried, G. A. Lagoda, A. Hristov, Y. Chuang, A. L. Burnett, and L. M. Su, "Optical coherence tomography of cavernous nerves: A step toward real-time intraoperative imaging during nerve-sparing radical prostatectomy," *Urology,* vol. 72, pp. 198-204, Jul 2008.

[35] M. Mayeh and F. Farahi, "Tailoring Gaussian Laser Beam Shape Through Controlled Etching of Single-Mode and Multimode Fibers: Simulation and Experimental Studies," *Ieee Sensors Journal,* vol. 12, pp. 168-173, Jan 2012.

[36] B. A. F. Puygranier and P. Dawson, "Chemical etching of optical fibre tips - experiment and model," *Ultramicroscopy,* vol. 85, pp. 235-248, Dec 2000.

[37] S. Mononobe and M. Ohtsu, "Fabrication of a pencil-shaped fiber probe for near-field optics by selective chemical etching," *Journal of Lightwave Technology,* vol. 14, pp. 2231-2235, Oct 1996.

[38] A. J. Welch, J. H. Torres, and W. F. Cheong, "Laser Physics and Laser-Tissue Interaction," *Texas Heart Institute Journal,* vol. 16, pp. 141-149, 1989.

[39] V. Knappe, F. Frank, and E. Rohde, "Principles of lasers and biophotonic effects," *Photomed Laser Surg,* vol. 22, pp. 411-7, Oct 2004.

[40] L. Carroll and T. R. Humphreys, "LASER-tissue interactions," *Clin Dermatol,* vol. 24, pp. 2-7, Jan-Feb 2006.

[41] J. A. Parrish and J. T. Walsh, Jr., "Potentials for progress in laser medicine," *Yale J Biol Med,* vol. 58, pp. 535-45, Nov-Dec 1985.

[42] J. Wells, C. Kao, P. Konrad, T. Milner, J. Kim, A. Mahadevan-Jansen, and E. D. Jansen, "Biophysical mechanisms of transient optical stimulation of peripheral nerve," *Biophysical Journal,* vol. 93, pp. 2567-2580, Oct 2007.

[43] P. Cesare, A. Moriondo, V. Vellani, and P. A. McNaughton, "Ion channels gated by heat," *Proceedings of the National Academy of Sciences of the United States of America,* vol. 96, pp. 7658-7663, Jul 6 1999.

[44] J. Wells, C. Kao, P. Konrad, A. Mahadevan-Jansen, and E. D. Jansen, "Photobiological mechanisms in optical stimulation of neural tissue," *Lasers in Surgery and Medicine,* pp. 10-10, Mar 2005.

[45] A. D. Izzo, J. T. Walsh, E. D. Jansen, M. Bendett, J. Webb, H. Ralph, and C. P. Richter, "Optical parameter variability in laser nerve stimulation: A study of pulse duration, repetition rate, and wavelength," *IEEE Transactions on Biomedical Engineering,* vol. 54, pp. 1108-1114, Jun 2007.

[46] A. D. Izzo, J. T. Walsh, H. Ralph, J. Webb, M. Bendett, J. Wells, and C. P. Richter, "Laser stimulation of auditory neurons: Effect of shorter pulse duration

and penetration depth," *Biophysical Journal,* vol. 94, pp. 3159-3166, Apr 15 2008.

[47] R. G. McCaughey, C. Chlebicki, and B. J. F. Wong, "Novel Wavelengths for Laser Nerve Stimulation," *Lasers in Surgery and Medicine,* vol. 42, pp. 69-75, Jan 2010.

[48] D. M. Quinlan, R. J. Nelson, A. W. Partin, J. L. Mostwin, and P. C. Walsh, "The Rat as a Model for the Study of Penile Erection," *Journal of Urology,* vol. 141, pp. 656-661, Mar 1989.

[49] http://www.nycrobotics.com.

[50] F. C. Henriques and A. R. Moritz, "Studies of Thermal Injury .1. The Conduction of Heat to and through Skin and the Temperatures Attained Therein - a Theoretical and an Experimental Investigation," *American Journal of Pathology,* vol. 23, pp. 531-&, 1947.

[51] C. Sramek, Y. Paulus, H. Nomoto, P. Huie, J. Brown, and D. Palanker, "Dynamics of retinal photocoagulation and rupture," *Journal of Biomedical Optics,* vol. 14, May-Jun 2009.

[52] J. T. Beckham, M. A. Mackanos, C. Crooke, T. Takahashi, C. O'Connell-Rodwell, C. H. Contag, and E. D. Jansen, "Assessment of cellular response to thermal laser injury through bioluminescence imaging of heat shock protein 70," *Photochemistry and Photobiology,* vol. 79, pp. 76-85, Jan 2004.

[53] M. S. Breen, M. Breen, K. Butts, L. L. Chen, G. M. Saidel, and D. L. Wilson, "MRI-guided thermal ablation therapy: Model and parameter estimates to predict cell death from MR thermometry images," *Annals of Biomedical Engineering,* vol. 35, pp. 1391-1403, Aug 2007.

[54] A. J. Welch and G. D. Polhamus, "Measurement and Prediction of Thermal-Injury in the Retina of the Rhesus-Monkey," *Ieee Transactions on Biomedical Engineering,* vol. 31, pp. 633-644, 1984.

[55] B. Chen, S. L. Thomsen, R. J. Thomas, J. Oliver, and A. J. Welch, "Histological and modeling study of skin thermal injury to 2.0 mu m laser irradiation," *Lasers in Surgery and Medicine,* vol. 40, pp. 358-370, Jul 2008.

[56] D. M. Simanovskii, M. A. Mackanos, A. R. Irani, C. E. O'Connell-Rodwell, C. H. Contag, H. A. Schwettman, and D. V. Palanker, "Cellular tolerance to pulsed hyperthermia," *Physical Review E,* vol. 74, Jul 2006.

[57] P. A. Garcia, J. H. Rossmeisl, R. E. Neal, T. L. Ellis, and R. V. Davalos, "A Parametric Study Delineating Irreversible Electroporation from Thermal Damage Based on a Minimally Invasive Intracranial Procedure," *Biomedical Engineering Online,* vol. 10, Apr 30 2011.

[58] X. M. He and J. C. Bischof, "The kinetics of thermal injury in human renal carcinoma cells," *Annals of Biomedical Engineering,* vol. 33, pp. 502-510, Apr 2005.

[59] Y. C. Wu, "A modified criterion for predicting thermal injury," *Nat Bur Stand.,* vol. Washington, District of Columbia, 1982.

[60] A. Takata, "Development of Criterion for Skin Burns," *Aerospace Medicine,* vol. 45, pp. 634-637, 1974.